Order by virtual crystal field fluctuations in pyrochlore XY antiferromagnets

Jeffrey G. Rau,[1] Sylvain Petit,[2] and Michel J. P. Gingras[1,3,4,5,6]

[1]*Department of Physics and Astronomy, University of Waterloo, Waterloo, Ontario N2L 3G1, Canada*
[2]*CEA, Centre de Saclay, DSM/IRAMIS/Laboratoire Leon Brillouin, F-91191 Gif-sur-Yvette, France*
[3]*Perimeter Institute for Theoretical Physics, Waterloo, Ontario N2L 2Y5, Canada*
[4]*Canadian Institute for Advanced Research, 180 Dundas Street West, Suite 1400, Toronto, Ontario M5G 1Z8, Canada*
[5]*Quantum Matter Institute, University of British Columbia, Vancouver, British Columbia V6T 1Z4, Canada*
[6]*TRIUMF, Theory Group, 4004 Wesbrook Mall, Vancouver, British Columbia V6T 2A3, Canada*

(Received 18 September 2015; published 10 May 2016)

Conclusive evidence of order by disorder is scarce in real materials. Perhaps one of the strongest cases presented has been for the pyrochlore XY antiferromagnet $Er_2Ti_2O_7$, with the ground state selection proceeding by order by disorder induced through the effects of quantum fluctuations. This identification assumes the smallness of the effect of virtual crystal field fluctuations that could provide an alternative route to picking the ground state. Here we show that this order by virtual crystal field fluctuations is not only significant, but competitive with the effects of quantum fluctuations. Further, we argue that higher-multipolar interactions that are generically present in rare-earth magnets can dramatically enhance this effect. From a simplified bilinear-biquadratic model of these multipolar interactions, we show how the virtual crystal field fluctuations manifest in $Er_2Ti_2O_7$ using a combination of strong-coupling perturbation theory and the random-phase approximation. We find that the experimentally observed ψ_2 state is indeed selected and the experimentally measured excitation gap can be reproduced when the bilinear and biquadratic couplings are comparable while maintaining agreement with the entire experimental spin-wave excitation spectrum. Finally, we comment on possible tests of this scenario and discuss implications for other order-by-disorder candidates in rare-earth magnets.

DOI: 10.1103/PhysRevB.93.184408

I. INTRODUCTION

The study of frustrated magnetism has led to the discovery of several new and exotic phenomena [1]. Much of this physics can be traced back to frustration inducing a large number of degenerate or nearly degenerate low-energy states, with the ultimate ground state and low energy physics being sensitive to subtle effects that act within this manifold. Due to this degeneracy, the relevant energy scales are then much smaller than in conventional unfrustrated systems and thus may arise from a wider variety of sources. The competition between the small interactions can lead to a rich set of phases, from unconventional magnetically ordered states to novel nonmagnetic phases such as classical or quantum spin liquids [1–3].

A particularly interesting class of degeneracy lifting mechanisms is *order by disorder*. In the seminal incarnations of Villain *et al.* [4] and Shender [5], thermal or quantum fluctuations, respectively, select the states from the degenerate manifold that have the largest space to fluctuate. This perspective naturally leads to a generalization of the idea of order by disorder, i.e., the selection from a degenerate manifold via any set of fluctuation corrections to the free energy. This mechanism of fluctuation induced order is not only a concept within the purview of frustrated magnetism, or even condensed matter physics taken more broadly, but even appears in high-energy physics in the guise of the Coleman-Weinberg mechanism [6]. This stabilization of order by quantum fluctuations, or *order by quantum disorder* [5,7,8], has an even longer history. While largely unnoticed, one of the earliest examples was put forth by Tessman [9] where quantum zero-point fluctuations select the magnetization direction in a dipolar ferromagnet [10,11].

More formally, we consider a system whose ordering is described by some order parameter m. The natural low-energy description can then be framed in terms of the effective action $\Gamma[m]$. In each order by disorder scenario, one starts from an artificial limit where there is an accidental degeneracy; that is, the effective action at this point, $\Gamma_0[m]$, has an accidental symmetry. For order by thermal disorder this limit is $T \to 0$, while for order by quantum disorder this is the classical limit where the spin becomes large, or $1/S \to 0$. Adding such perturbations moves the theory away from this artificial limit, adding a term $\delta\Gamma[m]$ to the effective action as $\Gamma[m] = \Gamma_0[m] + \delta\Gamma[m]$. A distinction is usually drawn between energetic and fluctuation-driven contributions to selection, i.e., between zeroth-order and higher-order perturbative corrections to $\delta\Gamma[m]$, though this can be somewhat ambiguous. Generically, $\delta\Gamma[m]$ breaks the accidental symmetry, lifting the degeneracy present in $\Gamma_0[m]$. In real systems such a $\delta\Gamma[m]$ correction should always be present, so long as the symmetry is not exact, with each order by disorder mechanism providing its own contribution to $\delta\Gamma[m]$. The identification of an order by disorder mechanism then relies not only on a proximity to the idealized $\Gamma_0[m]$ limit but also on the contribution of that mechanism to $\delta\Gamma[m]$ being dominant over all other sources of $\delta\Gamma[m]$ corrections. Beyond having just a single dominant order by disorder channel, these fluctuation selection mechanisms could thus cooperate and select the same state, or perhaps compete and prefer different states [4,7]. Competing order by disorder can lead to exotic multiple-step phase transitions, an unusual sensitivity to perturbations, or a host of other interesting properties.

While it is easy for deviations from the initial idealized limit to spoil an order by disorder selection mechanism, there are many systems where the simplest energetic selection mechanisms can be forbidden on fairly general grounds. Indeed, some of the early examples [5,9] focus on selection

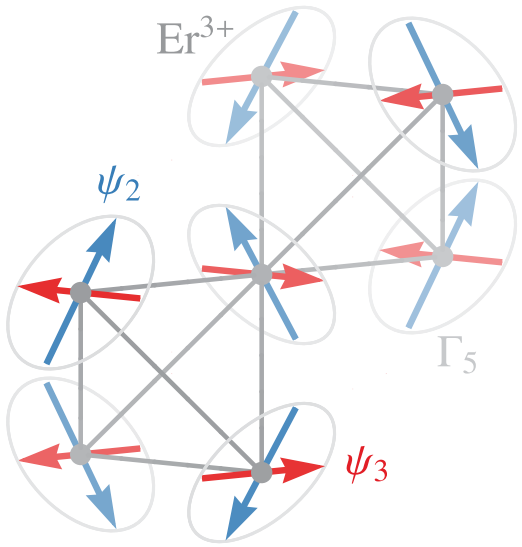

FIG. 1. In $Er_2Ti_2O_7$ the Er^{3+} ions form a pyrochlore lattice of corner-shared tetrahedra. The circles illustrate the allowed orientations in the ground state Γ_5 manifold, with the ψ_2 state (blue) and the ψ_3 state (red) indicated. The ψ_2 state is observed experimentally below 1.2 K.

of the moment direction in simple ferromagnets and antiferromagnets with high symmetry. Classically, the presence of three-, four-, or sixfold rotations axes can forbid the selection of a moment orientation purely from exchange anisotropy. In low-spin systems without sufficient single-ion anisotropy, the leading anisotropy then must come from effective multispin interactions. These can be generated at the level of a Landau-Ginzburg theory through the order by disorder mechanisms discussed above, be it thermal, quantum, or otherwise. To find a clear demonstration of this physics the challenge is then to find a material that is sufficiently close to such a limit with accidental ground state degeneracy. Theoretical and experimental control are essential: one must be able to characterize and quantify deviations from the idealized theoretical limit with the degeneracy while experimentally, one must be able to validate the theoretical model and approach the limiting regime closely, removing any extrinsic complications.

The class of rare-earth pyrochlore magnets $R_2M_2O_7$ are promising toward this goal [3,12]. Aside from having the requisite high symmetry, many are well described by an effective spin-1/2 model [13–15] and thus lack any on-site anisotropy. At the nearest-neighbor level, there are four symmetry allowed exchanges [16] leading to a diverse phase diagram that includes a variety of magnetic and nonmagnetic phases [17,18]. Included in this phase diagram is a large region where the effective spins order uniformly within their local XY planes [19]. This so-called Γ_5 manifold (see Fig. 1) can be thought of as a local ferromagnet and enjoys the degeneracy protection [15] discussed above. Of these rare-earth pyrochlores, we will focus on the titanate $Er_2Ti_2O_7$ which is close to ideal in each of these regards, having long been proposed as a prime example of order by disorder [20].

Experimentally, the thermodynamic properties of $Er_2Ti_2O_7$ are uncontroversial and have been well characterized. The Er^{3+} free ion hosts a $J = 15/2$ manifold that is quenched by the crystal field into an effective spin-1/2 degree of freedom with a strong planar (XY) anisotropy [20]. The low-lying crystal field energy levels have been measured to fair precision [20] and match well with theoretical models [21,22]. Ordering occurs near $T_N \sim 1.2$ K into the so-called ψ_2 state (see Fig. 1), a noncoplanar antiferromagnet [20,23]. The magnetic excitations above this state are sharp and have been measured across many cuts in reciprocal space via inelastic neutron scattering [15,24,25]. A nearly gapless mode is observed [24–26], suggesting a quasidegenerate set of ground states, as needed for order by disorder. Further, crystals of $Er_2Ti_2O_7$ can be made very clean, and disorder can be reintroduced in a controlled manner via depletion or stuffing [27]. The appropriate theoretical model of the effective spin-1/2 degrees of freedom has been tightly constrained by matching to the experimental data, through fitting of the inelastic neutron scattering spectrum in both zero and finite magnetic fields [15,25]. Altogether, this model can reproduce nearly all of the current experimental data at a qualitative and sometimes even a quantitative level [28].

Classically, this effective spin-1/2 model has an accidental degeneracy, the Γ_5 manifold mentioned above, consistent with the soft mode seen experimentally. Similarly, conventional mean-field theory shows the same accidental degeneracy in the Landau-Ginzburg theory near T_N [29]. This classical degeneracy remains unbroken for any symmetry allowed, two-spin interactions between the spins to arbitrary distance [15]. Several proposals on how to lift this degeneracy have been put forth; these include order by thermal disorder (for $T \to 0^+$ or $T \to T_c^-$) [20,29–32], order by quantum disorder [15,19,30,31], or order by structural disorder [33,34]. A case has been made for order by quantum disorder [15,31] as the operant mechanism in lifting the degeneracy of the classical ground state manifold in $Er_2Ti_2O_7$, with order by thermal disorder [28] cooperating at the ordering temperature T_N. A key prediction of the order by quantum disorder proposal is a gap in the excitation spectrum of order $\sim$20 μeV, comparable to the $\sim$40–45 μeV gap that was later observed experimentally [25,26]. One implicit limit that has been taken in all these studies is to assume that an effective spin-1/2 model with only two-spin interactions is itself sufficient. This can justified if one can take the crystal field energy scale η to be much larger than the exchange scale. Taking η to be finite then allows for corrections to the effective spin-1/2 model through virtual crystal field excitations, yet another channel contributing to $\delta\Gamma[m]$ as defined above. While these terms [25,35] have been argued to be extremely small [15], the complexity of the multipolar interactions between rare-earth ions [36–39] and the subtleties arising from the combinatorics of high-order perturbation theory demand a more careful accounting of these effects.

In this article, we aim to carefully address the effects of virtual crystal field fluctuations [25,35] on the ground state selection in $Er_2Ti_2O_7$. We find that such an *order by virtual crystal field fluctuations* is not only significant, but is naturally comparable with the effects from order by quantum disorder. When mapped into the effective spin-1/2 description via strong-coupling perturbation theory, these fluctuations manifest as multispin interactions, with a complementary interpretation as classical energetic selection. We argue that the

complex multipolar interactions that exist in the full $J = 15/2$ manifold further enhance these fluctuations, compared to the case of only bilinear interactions between the angular momenta $\mathbf{J}$, and render them very relevant in describing $Er_2Ti_2O_7$. For definiteness, we consider a bilinear-biquadratic exchange model of the $J = 15/2$ moments as a minimal model of this physics. We analyze the effects of virtual crystal field fluctuations using a combination of mean-field theory (MFT) and random-phase approximation (RPA) calculations. We show that these MFT+RPA calculations are qualitatively consistent with a treatment of the multispin interactions via strong-coupling perturbation theory, and thus capture the effects of the virtual crystal field excitations. Generically, we find that this mechanism is cooperative with thermal and quantum selection, selecting the ψ_2 state as is seen experimentally. From these calculations we find that when the bilinear and biquadratic couplings are comparable this selection mechanism can be of similar magnitude or even dominate over the effects of order by quantum disorder [15,31]. We thus conclude that $Er_2Ti_2O_7$ may not ultimately be the long sought definite case for order by quantum disorder controlling ground state selection. More broadly, we have identified an important fluctuation channel in rare-earth magnets, which highlights some of the pitfalls that can may be hidden in the effective spin-1/2 theory. Knowledge of the leading mechanisms for ground state selection is important in the search for candidates that realize order by disorder. While cooperative in $Er_2Ti_2O_7$, similar considerations may yield competing mechanisms for state selection in other materials, with associated multiple phase transitions or other exotic behaviors. Finally, we discuss how these considerations may apply to other materials in this family, such as the pyrochlore magnets $Er_2M_2O_7$ or $Yb_2M_2O_7$.

The paper is organized as follows: We begin Sec. II by reviewing the low-energy effective spin-1/2 model for $Er_2Ti_2O_7$. We then show in Sec. II A and Sec. II B how this effective model arises from underlying multipolar interactions between the $J = 15/2$ manifolds of the Er^{3+} ions, and discuss the generation of multispin interactions by virtual crystal field fluctuations. We build on this in Sec. III, showing how these multispin interactions lead to ground state selection and order by virtual crystal field fluctuations. In Sec. III A, we show how this selection proceeds and how it is related to the gap in the spin-wave spectrum, presenting estimates for their magnitude in Sec. III B. Next, in Sec. IV, we perform an explicit calculation of these quantities for two models of multipolar interactions in $Er_2Ti_2O_7$. As discussed in Sec. IV A and Sec. IV B, these models include both bilinear and biquadratic exchange, and are solved with the RPA approximation as outlined in Sec. IV C. The results for ground state selection and the excitation spectrum are presented in Sec. V. The application of these results to $Er_2Ti_2O_7$ and how to disentangle different order by disorder scenarios are discussed in Sec. VI. Finally, we comment in Sec. VII on possible implications for other materials.

II. EFFECTIVE MODELS

Before delving into the detailed modeling of $Er_2Ti_2O_7$, we first summarize the arguments that lead to the effective spin-1/2 model that has been used in prior works [15,28]. The ground state of the free Er^{3+} ion consists of the $^4I_{15/2}$ manifold of the $4f^{11}$ electronic configuration which carries a $J = 15/2$ moment. In the pyrochlore structure of $Er_2Ti_2O_7$ (space group $Fd\bar{3}m$), the Er^{3+} ion lies at a site with D_{3d} symmetry. The crystal field lifts the degeneracy of the $^4I_{15/2}$ manifold, splitting it into a set of effective spin-1/2 Γ_4 doublets and dipolar-octupolar $\Gamma_5 \oplus \Gamma_6 \equiv \Gamma_{56}$ doublets [40]. The ground doublet is an effective spin-1/2 degree of freedom of type Γ_4 with a gap of $\Lambda \sim 6$ meV ($\sim$70 K) to the first excited state [20]. Since this energy scale is large relative to the exchanges, which are expected to be $\sim$0.1 K to 1 K [15,25], it is justified to consider an effective spin-1/2 model, down-folding the full set of crystal field levels into the ground doublet defined as $|\pm\rangle$. In the coarsest approximation, one simply projects the $J = 15/2$ moment $\mathbf{J}_i$ at site $\mathbf{r}_i$ into this manifold,

$$P\mathbf{J}_i P = \lambda_\pm\left(S_i^x\hat{\mathbf{x}} + S_i^y\hat{\mathbf{y}}\right) + \lambda_z S_i^z\hat{\mathbf{z}} \equiv \boldsymbol{\lambda}\mathbf{S}_i, \tag{1}$$

where $\mathbf{S}_i$ is the effective spin-1/2 operator and $\boldsymbol{\lambda} \equiv \mathrm{diag}(\lambda_\pm,\lambda_\pm,\lambda_z)$ with $\lambda_\pm \sim 6$ and $\lambda_z \sim 2$ depends on the details of the crystal field parameters through the spectral composition of the ground doublet. These λ factors are related to the g factors which characterize the response to an applied magnetic field via $\lambda_\mu = g_\mu/g_J$ where $\mu = \pm,z$ and $g_J = 6/5$ is the Landé factor for Er^{3+}. Both the $\mathbf{J}_i$ and $\mathbf{S}_i$ operators are defined in the local basis $(\hat{\mathbf{x}}_i,\hat{\mathbf{y}}_i,\hat{\mathbf{z}}_i)$ defined with respect to the high-symmetry directions at each site, as defined in Appendix A. In this local picture, the Γ_5 manifold corresponds to ferromagnetic ordering in the local XY plane, with ψ_2 defined as the moments ordered in the local $\hat{\mathbf{x}}$ direction (see Fig. 1). The remaining states can be obtained from ψ_2 by a rotation of all the spins about their local [111] direction.

As discussed in the Introduction, the most detailed information on the interactions with the Er^{3+} ions comes from fitting such an effective spin-1/2 model to the results of inelastic neutron scattering experiments [15,25]. It was found that a model with only nearest-neighbor anisotropic exchange between the effective spin-1/2 moments provides a fairly good description of the observed spectrum. By symmetry, the effective spin-1/2 Hamiltonian takes the form [15,16]

$$\begin{aligned} H_{\mathrm{eff}} = \sum_{\langle ij\rangle}\mathbf{S}_i^{\intercal}\boldsymbol{\mathcal{J}}_{ij}\mathbf{S}_j \equiv \sum_{\langle ij\rangle}\Big\{&\mathcal{J}_{zz}S_i^zS_j^z - \mathcal{J}_\pm\left(S_i^+S_j^- + S_i^-S_j^+\right) \\ &+ \mathcal{J}_{\pm\pm}\left(\gamma_{ij}S_i^+S_j^+ + \mathrm{H.c.}\right) + \mathcal{J}_{z\pm}\left(\zeta_{ij}\left[S_i^zS_j^+ + S_i^+S_j^z\right]\right. \\ &\left.+\mathrm{H.c.}\right)\Big\}. \end{aligned} \tag{2}$$

Details of the complex form factors γ_{ij} and ζ_{ij} are given in Appendix A. From experimental fitting [15,25], the $\mathcal{J}_{ij}$ couplings are of order 10^{-2} meV with $\mathcal{J}_\pm$ and $\mathcal{J}_{\pm\pm}$ being the largest. A representative example, from Ref. [15], is

$$\begin{aligned} &\mathcal{J}_{zz} = -2.5\times10^{-2}\ \mathrm{meV}, \quad \mathcal{J}_\pm = +6.5\times10^{-2}\ \mathrm{meV}, \\ &\mathcal{J}_{\pm\pm} = +4.2\times10^{-2}\ \mathrm{meV}, \quad \mathcal{J}_{z\pm} = -0.88\times10^{-2}\ \mathrm{meV}. \end{aligned} \tag{3}$$

Further details on other proposed sets of effective spin-1/2 exchanges are found in Appendix B 2. Longer range couplings, such as second or third neighbor exchanges or dipolar interactions, are generally expected to be present, but have not been found to be necessary to reproduce the features that are theoretically accessible within current experimental uncertainties. While this model has been found to be fairly

successful, we show, as outlined in the Introduction, that higher corrections that go beyond the coarse approximation encapsulated in Eq. (2) will prove to be significant. To include such corrections, we must build a model for $Er_2Ti_2O_7$ starting from the higher energy atomic physics and progressing towards the low-energy effective Hamiltonian.

A. Multipolar interactions

The structure of the model (2) was essentially fixed by symmetry and the restriction to only two-spin (bilinear) interactions between the effective spin-1/2 degrees of freedom. Information on the microscopic interactions between the $\mathbf{J}_i$ moments or the $4f$ electrons themselves is essentially lost through the projection into the ground doublets, compressed into the four exchange parameters $\mathcal{J}_{zz}, \mathcal{J}_{\pm}, \mathcal{J}_{\pm\pm}$, and $\mathcal{J}_{z\pm}$. To go beyond this projection into the ground doublets, we move up in energy and consider a model of the multipolar interactions between the $J = 15/2$ moments. As above, we consider only interactions between nearest-neighbor sites. This can be partially justified as, aside from the long-range dipolar interactions, one expects multipolar couplings to arise from short-range superexchange type processes [36,37].

In contrast to the effective spin-1/2 model of Eq. (2), we do not expect these more microscopic interactions to have only a bilinear form. Unlike the effective spin-1/2 moments, the $J = 15/2$ manifolds of the Er^{3+} ions can support many higher-order multipoles. These multipoles can be classified into *ranks*; the familiar dipole operators $\sim J^\alpha$ are rank 1, quadrupole operators $\sim J^\alpha J^\beta$ are rank 2, and so forth. As $J = 15/2$, such multipoles can be constructed up to and including rank 15. To proceed in a systematic fashion we introduce a basis for these multipole operators that transforms in the same way as the spherical harmonics. As for the spherical harmonics, for a rank-K multipole we have $2K + 1$ operators indexed by $Q = -K, -K+1, \ldots, +K-1, +K$. More explicitly, we define the set of rank-K multipoles $O_{KQ}(\mathbf{J})$

$$\langle J,M|O_{KQ}(\mathbf{J})|J,M'\rangle \equiv \sqrt{\frac{2K+1}{2J+1}}\langle J,M;K,-Q|J,M'\rangle, \tag{4}$$

where $\langle J,M;K,-Q|J,M'\rangle$ is a Clebsch-Gordan coefficient and $|J,M\rangle$ are eigenstates of $\mathbf{J}\cdot\mathbf{J}$ and J^z. These operators have been normalized so that $\mathrm{tr}[O_{KQ}(\mathbf{J})^\dagger O_{KQ}(\mathbf{J})] = 1$, so the different ranks can be compared on equal footing without worrying about large matrix element factors that arise when acting on the $|J,M\rangle$ states. The rank-1 vector operators are then simply a reformulation of the dipole moment $\mathbf{J}_i$,

$$O_{1,0}(\mathbf{J}) = \frac{1}{2\sqrt{85}}J^z, \quad O_{1,\pm1}(\mathbf{J}) = \pm\frac{1}{2\sqrt{85}}\left(\frac{J^x \pm iJ^y}{\sqrt{2}}\right), \tag{5}$$

where the factor of $1/(2\sqrt{85})$ enforces the trace normalization. We note that these operators are similar to, but not identical to, the Stevens' operator equivalents [41] used to define the crystal field potential.

With these degrees of freedom in hand, we can write down a model of their interactions. Aside from the crystal field potential, because of the weakness of superexchange processes in $4f$ insulators [37] we expect them to be predominantly pair-wise, generically giving the model

$$\sum_{\langle ij\rangle}\sum_{KQ}\sum_{K'Q'} O_{KQ}(\mathbf{J}_i)\mathcal{M}_{ij}^{KQ,K'Q'}O_{K'Q'}(\mathbf{J}_j) + \sum_i \mathcal{V}(\mathbf{J}_i), \tag{6}$$

where $\mathcal{V}(\mathbf{J})$ is the crystal field potential, $O_{KQ}(\mathbf{J}_i)$ is a multipole of rank K, and $\boldsymbol{\mathcal{M}}$ are the multipolar coupling constants. The form and parameters we use for $\mathcal{V}(\mathbf{J})$ are discussed in Appendix B 1. Processes such as superexchange can only generate interactions up to including rank-7 multipoles [36–39]. Given that the anisotropy in the fitted exchanges in $Er_2Ti_2O_7$ deviates strongly from that expected from magnetostatic dipolar interactions, we expect the superexchange scale to be significant, and thus a wide range of multipolar ranks to be present in the interactions of the $J = 15/2$ model given by Eq. (6). There are an enormous number of independent couplings embedded in the matrix $\boldsymbol{\mathcal{M}}$, given that $K, K' \leqslant 7$ and $|Q| \leqslant K, |Q'| \leqslant K'$. Even accounting for symmetry leaves hundreds of possible couplings. Thankfully, we have some semblance of a separation of scales via the crystal field potential, which at $\Lambda \sim 6$ meV is roughly two orders of magnitude larger than the expected scale for $\mathcal{M}$.

We now have all the pieces to improve on the effective model of Eq. (2), which can, in principle, be obtained for a given $\boldsymbol{\mathcal{M}}$ by a bare projection of Eq. (6) into the ground doublets. In the following section we sketch a derivation of the low-energy effective model that goes beyond simply the bilinear interactions defined in Eq. (2). We do this leaving the multipolar interactions somewhat arbitrary, relegating the detailed discussion of their form to Sec. IV.

B. Strong-coupling perturbation theory

To derive the low-energy effective model, we carry out strong-coupling perturbation theory in the crystal field potential, perturbing with the multipolar couplings. Aside from the simple model of Eq. (2), we also consider the higher order corrections that have been ignored in previous studies. More concretely, we use the Rayleigh-Schrödinger perturbation theory as presented in Lindgren [42]. We decompose the full Hamiltonian, H, as $H = \eta H_0 + V$, where

$$H_0 = \sum_i \mathcal{V}(\mathbf{J}_i), \tag{7a}$$

$$V = \sum_{\langle ij\rangle}\sum_{KQ}\sum_{K'Q'} O_{KQ}(\mathbf{J}_i)\mathcal{M}_{ij}^{KQ,K'Q'}O_{K'Q'}(\mathbf{J}_j). \tag{7b}$$

To control the passage from the $J = 15/2$ model to the effective spin-1/2, we have added a dimensionless rescaling parameter η to the crystal field. The choice $\eta = 1$ corresponds to the physical, experimentally fitted crystal field Hamiltonian [22], with larger values suppressing the effects (i.e., admixing) of the higher lying crystal field doublets in the low-energy sector composed of the ground doublets. The bare Hamiltonian ηH_0 is diagonalized using single-ion crystal field states at each site. To proceed with the perturbation theory, we define a projector into the ground state manifold, $P = \sum_{E_n=E_0}|n\rangle\langle n|$, along with a resolvent operator

$$R = \sum_{E_n\neq E_0}\frac{|n\rangle\langle n|}{E_0 - E_n}, \tag{8}$$

where E_n and $|n\rangle$ are the eigenvalues and eigenstates of H_0. This perturbation theory becomes formally exact in the limit $\eta \to \infty$. The expansion of the effective Hamiltonian is given in Lindgren [42] as $H_{\rm eff} = \sum_n \eta^{-n+1} H_{{\rm eff},n}$. Here one considers a wave operator, Ω, related to the effective Hamiltonian as $H_{\rm eff} = PV\Omega$ with the analogous expansion $\Omega = \sum_n \eta^{-n+1}\Omega_n$. These are defined via the relation

$$\Omega_n = RV\Omega_{n-1} - R\sum_{m=1}^{n-1} \Omega_{n-m} V \Omega_{m-1}. \tag{9}$$

Starting with $\Omega_1 = P$, the higher order Ω_n, and thus $H_{{\rm eff},n}$, can be computed recursively. The first three orders are given by

$$H_{{\rm eff},1} = PVP, \tag{10a}$$
$$H_{{\rm eff},2} = PVRVP, \tag{10b}$$
$$H_{{\rm eff},3} = PVRVRVP - \tfrac{1}{2}\{(PVR^2VP), PVP\}, \tag{10c}$$

where $\{\cdot,\cdot\}$ is the anticommutator [43]. Due to their complexity, we will not give the expressions for $H_{{\rm eff},4}$ and $H_{{\rm eff},5}$, but they can be straightforwardly computed from Eq. (9).

The leading term, $H_{{\rm eff},1}$, is simply the projection of the multipolar interactions, V, into the ground doublets. This can be accomplished by projecting the multipoles individually,

$$PO_{KQ}(\mathbf{J}_i)P = \begin{cases} \mathbf{v}_{KQ}\cdot\mathbf{S}_i & \text{if } K \text{ odd}, \\ \text{const.} & \text{if } K \text{ even}, \end{cases} \tag{11}$$

then substituting them back into V in Eq. (6). The vectors $\mathbf{v}_{KQ}$ are in general complex and define the mapping into the effective spin-1/2, depending only on the spectral composition of the ground doublet. At first order in perturbation theory, the even-rank terms lead only to a constant shift of the energy and can be ignored. As such, we see that the even-rank multipolar interactions are *completely unconstrained* by the fitted effective spin-1/2 exchanges, $\mathcal{J}_{ij}$. Combined together, the odd terms give the interactions between the effective spin-1/2 operators $\mathbf{S}_i$ as

$$H_{{\rm eff},1} = \sum_{\langle ij\rangle} \mathbf{S}_i^{\intercal}\Big(\sum_{KQ}\sum_{K'Q'} \mathbf{v}_{KQ}\mathbf{v}_{K'Q'}^{\intercal}\mathcal{M}_{ij}^{KQ,K'Q'}\Big)\mathbf{S}_j. \tag{12}$$

This leads to the symmetry allowed nearest-neighbor model as given in Eq. (2), with only two-spin interactions, where the tremendous complexity of $\boldsymbol{\mathcal{M}}$ is embedded in the four symmetry allowed exchanges $\mathcal{J}_{zz}, \mathcal{J}_{\pm}, \mathcal{J}_{\pm\pm}$, and $\mathcal{J}_{z\pm}$.

At higher order, further corrections will be generated through virtual crystal field fluctuations [44] involving the excited single-ion states through the resolvent operators that appear in Eq. (10). The leading corrections that do not simply renormalize the bilinear couplings are four- and six-spin interactions [19,29] which appear at third and fifth order in $\mathcal{M}$. We thus write the effective Hamiltonian at fifth order in three pieces, $H_{\rm eff} = H_2 + H_4 + H_6$, containing the two-, four-, and six-spin interactions. Explicitly, we have

$$H_2 = \sum_{i_1 i_2}\sum_{\alpha_1\alpha_2} \mathcal{J}_{i_1 i_2}^{\alpha_1\alpha_2} S_{i_1}^{\alpha_1} S_{i_2}^{\alpha_2}, \tag{13a}$$
$$H_4 = \sum_{i_1\cdots i_4}\sum_{\alpha_1\cdots\alpha_4} \mathcal{K}_{i_1\cdots i_4}^{\alpha_1\cdots\alpha_4} S_{i_1}^{\alpha_1} S_{i_2}^{\alpha_2} S_{i_3}^{\alpha_3} S_{i_4}^{\alpha_4}, \tag{13b}$$
$$H_6 = \sum_{i_1\cdots i_6}\sum_{\alpha_1\cdots\alpha_6} \mathcal{L}_{i_1\cdots i_6}^{\alpha_1\cdots\alpha_6} S_{i_1}^{\alpha_1} S_{i_2}^{\alpha_2} S_{i_3}^{\alpha_3} S_{i_4}^{\alpha_4} S_{i_5}^{\alpha_5} S_{i_6}^{\alpha_6}. \tag{13c}$$

The lowest order part of the bilinear couplings $\mathcal{J}$ in Eq. (13) are the nearest-neighbor projection of the multipolar interactions at order $\mathcal{M}$, as given in Eq. (12). Higher corrections at orders $\mathcal{M}^2/(\eta\Lambda)$ up to $\mathcal{M}^5/(\eta\Lambda)^4$ renormalize bilinear couplings between the effective spin-1/2 operators, as well as inducing second, third, and further neighbor exchanges where Λ defines the scale of crystal field when $\eta = 1$. The projection of the nearest-neighbor part will be taken to match the experimentally determined values of Eq. (3). The subleading further-neighbor exchanges do not lift the Γ_5 degeneracy on their own [15] and serve only to renormalize the bilinear exchange scale. While these corrections will modify the spin-wave dispersion and other features of model, it will not affect the ground state selection or excitation gap. Since this is our focus and the question of foremost interest, we ignore these terms.

The four-spin interactions, $\mathcal{K}$, appear first at order $\mathcal{M}^3/(\eta\Lambda)^2$ and receive subleading corrections from fourth and fifth order as $\mathcal{M}^4/(\eta\Lambda)^3$ and $\mathcal{M}^5/(\eta\Lambda)^4$. We keep only the leading terms, at order $\mathcal{M}^3/(\eta\Lambda)^2$, where the four sites $i_1,\ldots,i_4$ take the form of trees built from three nearest-neighbor bonds of the lattice. For example, a tree for three bonds can involve four distinct sites and thus contribute to the four-spin operators at order $\mathcal{M}^3/(\eta\Lambda)^2$. Contributions with three bonds that have a loop involve at most two or three spins and cannot contribute to a four-spin term. Similarly, for the six-spin interactions, $\mathcal{L}$, the leading contribution comes in at order $\mathcal{M}^5/(\eta\Lambda)^4$ with the sites $i_1,\ldots,i_6$ forming trees built from five nearest-neighbor bonds. A large number of possible anisotropic couplings are allowed through the dependence on the spin indices in both the four- and six-spin interaction terms.

III. ORDER BY VIRTUAL CRYSTAL FIELD FLUCTUATIONS

Having exposed how higher spin interactions are induced by virtual crystal field excitations, we next need to understand how the resulting four- and six-spin interactions affect the ground state selection and the energy gap. To do this, we construct a variational product state for each local ferromagnetic ordering direction $|\hat{\mathbf{n}}\rangle$ as

$$|\hat{\mathbf{n}}\rangle \equiv \prod_{i=1}^{N}\Big[\cos\frac{\theta}{2}|\uparrow\rangle_i + e^{i\phi}\sin\frac{\theta}{2}|\downarrow\rangle_i\Big], \tag{14}$$

where $|\uparrow\rangle_i, |\downarrow\rangle_i$ are effective spin-1/2 states of the low-energy effective model and (θ,ϕ) are the spherical angles for the direction $\hat{\mathbf{n}}$. By construction, the expectation value of the effective spin-1/2 is oriented in the direction specified by θ and ϕ:

$$\langle\hat{\mathbf{n}}|\mathbf{S}_i|\hat{\mathbf{n}}\rangle = \tfrac{1}{2}[\sin\theta(\cos\phi\hat{\mathbf{x}} + \sin\phi\hat{\mathbf{y}}) + \cos\theta\hat{\mathbf{z}}] = \tfrac{1}{2}\hat{\mathbf{n}}. \tag{15}$$

The Γ_5 manifold is then the set of states with $\theta = \pi/2$, ψ_2 corresponding to $\phi = n\pi/3$ and ψ_3 to $\phi = n\pi/3 + \pi/6$ with $n = 0,1,2,\ldots,5$.

When phrased in terms of the states in the low-energy effective model, the state $|\hat{\mathbf{n}}\rangle$ contains no intersite correlations. Thus when viewed through the lens of the low-energy effective model, the selection via multispin interactions could be regarded as a purely classical energetic effect. While intuitive, such a perspective obscures some of the key aspects of the physics. A more complete viewpoint requires consideration of what $|\hat{\mathbf{n}}\rangle$ corresponds to in terms of the physical $|\pm\rangle_i$ crystal field ground doublets. At zeroth-order one would simply map the effective spin-1/2 states into the ground doublets directly, replacing $|\uparrow\rangle_i \rightarrow |+\rangle_i$ and $|\downarrow\rangle_i \rightarrow |-\rangle_i$ in Eq. (14). At higher orders in perturbation theory the relationship between the states of the low-energy effective theory and the underlying $J = 15/2$ manifold becomes nontrivial. Following Lindgren [42], the $|\hat{\mathbf{n}}\rangle$ state maps to

$$|\hat{\mathbf{n}}\rangle_\Omega \equiv \Omega|\hat{\mathbf{n}}\rangle, \tag{16}$$

where Ω is the wave operator whose expansion was given in Eq. (9). The physical state $|\hat{\mathbf{n}}\rangle_\Omega$ is not a product state in the ground doublets $|\pm\rangle_i$. The wave operator Ω has much of the same structure as the effective Hamiltonian and is nonlocal in the moment operators $\mathbf{J}_i$. This mapping encodes nontrivial correlations between the sites, as well as virtual fluctuations into the higher crystal field levels.

The degeneracy lifting is thus induced through virtual fluctuations into the higher crystal field levels of the $J = 15/2$ manifold that are built into the state itself. We therefore refrain from referring to this ground state selection as "energetic" and thus call this mechanism *order by virtual crystal field fluctuations*. Most importantly, this is distinct from the correlations built into the state in the order by quantum disorder scenario [15]; the correlations induced here vanish as the crystal field energy scale becomes large, i.e., as $\eta \rightarrow \infty$.

Given this mapping, one may ask how the direction $\hat{\mathbf{n}}$ relates to direction of the physical moments $\mathbf{J}_i$. For the ψ_2 ($\phi = n\pi/3$) and ψ_3 ($\phi = n\pi/3 + \pi/6$) states of interest, this is partially constrained by their remnant symmetry. Each ψ_3 state is preserved (locally) by the C_2 rotation along the moment direction, while each ψ_2 state is preserved by a combination of a C_2 axis perpendicular to the moment, combined with time reversal. As the mapping Ω preserves the underlying space-group symmetries of the model, these remnant symmetries are also reflected in the expectations of the moments $\mathbf{J}_i$. This then implies that the local in-plane angle is preserved by Ω for the ψ_2 and ψ_3 states. We note that for ψ_3 the vanishing of the component out of the local [111] plane is also preserved with the expectation $\mathbf{J}_i$ remaining fixed in the local XY planes. For ψ_2, a finite canting out of the XY plane [29] is generically induced by this mapping, in addition to an intrinsic generation [see Eq. (22)] that will be discussed in the following section.

A. Selection and excitation gap

We can now look at the selection of the ψ_2 or ψ_3 state and the excitation gap that follows generically. Using the effective spin-1/2 language, we compute the energy per spin as

$$E(\hat{\mathbf{n}}) \equiv \langle \hat{\mathbf{n}}|H_{\text{eff}}|\hat{\mathbf{n}}\rangle/N. \tag{17}$$

Practically, one simply replaces each effective spin-1/2 operator in H_{eff} with the classical spin vector in Eq. (15), dividing by the total number of sites. The energy per spin is then given by

$$E(\hat{\mathbf{n}}) = C_2 \cos^2\theta + C_4 \cos\theta \sin^3\theta \cos 3\phi - C_6 \cos 6\phi, \tag{18}$$

where the overall form is dictated by symmetry constraints, as has been discussed in Refs. [19,29]. The C_n coefficients are determined by the exchanges in Eq. (13) and are given by

$$C_2 = \frac{1}{2}\sum_{i_1 i_2}\sum_{\alpha_1\alpha_2} \mathcal{J}^{\alpha_1\alpha_2}_{i_1 i_2}, \tag{19a}$$

$$C_4 = \frac{1}{2^4}\sum_{i_1\cdots i_4}\sum_{\alpha_1\cdots\alpha_4} \mathcal{K}^{\alpha_1\cdots\alpha_4}_{i_1\cdots i_4}, \tag{19b}$$

$$C_6 = \frac{1}{2^6}\sum_{i_1\cdots i_6}\sum_{\alpha_1\cdots\alpha_6} \mathcal{L}^{\alpha_1\cdots\alpha_6}_{i_1\cdots i_6}. \tag{19c}$$

At zeroth order in $1/\eta$, the C_2 coefficient can be worked out from the bare projected couplings with

$$C_2 \approx 3(\mathcal{J}_{zz} + 2\mathcal{J}_{\pm}). \tag{20}$$

The value of this coefficient does not depend too much on the choice of the exchange parameters; using the parameters of Ref. [15] one has $C_2 \sim 0.3 \pm 0.1$ meV, while from Ref. [25] one has $C_2 \sim 0.3 \pm 0.05$ meV. The contributions from the $\mathcal{J}_{\pm\pm}$ and $\mathcal{J}_{z\pm}$ terms cancel for local ferromagnetic states due to their complex form factors γ_{ij} and ζ_{ij} in Eq. (2). Such a cancellation is generic [15], as a by-product of lattice symmetries further guaranteeing that further bilinear interactions of arbitrary range do not lift the degeneracy of the Γ_5 manifold.

To see which state is selected, we minimize the total energy per spin, $E(\hat{\mathbf{n}})$, as a function of θ and ϕ. Given that the coefficient C_2 is positive and leading for the parameters relevant to $Er_2Ti_2O_7$, we expect predominantly in-plane order ($\theta \sim \pi/2$). We thus can expand about $\theta = \pi/2$ as

$$E(\hat{\mathbf{n}}) \sim C_2\left(\theta - \frac{\pi}{2}\right)^2 - C_4\left(\theta - \frac{\pi}{2}\right)\cos(3\phi) + \cdots, \tag{21}$$

where the omitted terms do not depend on θ. This gives a minimum at

$$\theta_0 = \frac{\pi}{2} + \left(\frac{C_4}{2C_2}\right)\cos(3\phi). \tag{22}$$

Fixing $\theta = \theta_0$ and using Eq. (18), the energy difference [45] between the ψ_2 and ψ_3 states is then

$$\delta E \equiv E(\psi_3) - E(\psi_2) = 2\left(\frac{C_4^2}{8C_2} + C_6\right). \tag{23}$$

If $C_4^2 + 8C_2C_6 > 0$, the ψ_2 states are selected and otherwise ψ_3 is selected. The ψ_2 ($\phi = n\pi/3$) states are modified by a small canting out of the local XY plane as indicated by $\theta_0 \neq \pi/2$ [29] in Eq. (22). One sees then that a nonzero C_4 always favors the selection of ψ_2 while a finite C_6 can select ψ_2 or ψ_3 depending on its sign. This can be seen in the absence of canting in the ψ_3 state where $\theta_0 = \pi/2$ for $\phi_0 = n\pi/3 + \pi/6$ in Eq. (22). Thus ψ_3 cannot gain any energy from the C_4 term and must be

stabilized solely by C_6. This may naively suggest that, within the order by virtual crystal field fluctuation scenario, selection of ψ_2 may be more prevalent in real materials.

Having identified how ψ_2 or ψ_3 are selected within the Γ_5 manifold, we estimate the size of the spin-wave gap in the ψ_2 state. Solving the classical equations of motion for a finite energy $\mathbf{k} = 0$ mode, the gap is given by [46]

$$\Delta = 2\sqrt{A_{\phi\phi}A_{\theta\theta} - A_{\theta\phi}^2}. \tag{24}$$

The $A_{\phi\phi}, A_{\theta\theta}$, and $A_{\theta\phi}$ are the curvatures of the classical energy, defined as

$$E(\hat{\mathbf{n}}) \sim \tfrac{1}{2}A_{\theta\theta}(\theta-\theta_0)^2 + \tfrac{1}{2}A_{\phi\phi}(\phi-\phi_0)^2 + A_{\theta\phi}(\theta-\theta_0)(\phi-\phi_0) + \cdots, \tag{25}$$

where ϕ_0 is taken to be zero for the ψ_2 state. The cross-term $A_{\theta\phi}$ vanishes, so the classical gap Δ is given by the geometric mean of the curvatures divided by the moment size [25,46] as in Eq. (24). Explicitly,

$$\Delta = 3\sqrt{C_4^2 + 8C_2C_6}. \tag{26}$$

In this form, we see from Eq. (23) that the energy difference, δE, between the ψ_3 and ψ_2 states and the gap size are related as

$$\Delta^2 = 36C_2\delta E. \tag{27}$$

We note that in the quantum order by disorder scenario [15], a similar relation is given for the order by quantum disorder gap as found in linear spin-wave theory, albeit with a different numerical prefactor. With the relationship of the multispin interactions to the energy difference and excitation gap in hand, we move on to derive estimates of the size of the four- and six-spin interactions C_4 and C_6.

B. Scaling arguments

While we have assumed that $|C_4|, |C_6| \ll C_2$, to understand whether these terms are competitive with other effects, such as order by quantum disorder, we need a more explicit estimate of their magnitude. First, we consider simple scaling arguments [15,25] for the size of these terms from the strong-coupling expansion sketched in Sec. II B. One has

$$C_2 \sim \mathcal{J}, \quad C_4 \sim \mathcal{J}^3/(\eta\Lambda)^2, \quad C_6 \sim \mathcal{J}^5/(\eta\Lambda)^4, \tag{28}$$

where $\boldsymbol{\mathcal{J}} = \boldsymbol{\lambda}^{-1}\boldsymbol{\mathcal{M}}\boldsymbol{\lambda}^{-1}$. The $\boldsymbol{\lambda}$ factors of size $\lambda_z \sim 2$ and $\lambda_\pm \sim 6$ provide an accounting for the size of the matrix elements of the $J = 15/2$ operators. From Eq. (26), the gap should then scale as $\Delta \sim \mathcal{J}^3/(\eta\Lambda)^2$ when a ψ_2 state has been stabilized. From the fitted exchanges [15,25], one has $\mathcal{J} \sim 0.01$–0.1 meV and $\Lambda \sim 6$ meV, so even optimistically it would seem that one would estimate a very small gap $\Delta \sim 0.001$–0.01 μeV via Eq. (26) and Eq. (28). This value is roughly in agreement with that argued in Ref. [15], and suggests that the virtual crystal field excitations are irrelevant to the ground state selection.

However, this is somewhat naïve, as it excludes significant combinatoric factors. To see this, consider the multipolar interactions in V on each nearest-neighbor bond as being independent perturbations to ηH_0, with $V \equiv \sum_{\langle ij\rangle} V_{ij}$. We then define a *contribution* to $H_{\text{eff,n}}$ as some string of $n-1$ resolvent operators R and n perturbations V_{ij}. These bonds must be connected and, for the leading contributions to C_4 and C_6, must form trees, i.e., have no loops. Any contribution to $H_{\text{eff,n}}$ with loops will involve less than n distinct sites and thus will not be the leading parts of the coefficient, as mentioned in Sec. II B. The number of contributions from three connected nearest-neighbor bonds of the pyrochlore lattice is of order 10^2 and from five connected nearest-neighbors is of order 10^3–10^4. Since each of these contributions is of order $\mathcal{J}$, the estimates given above should include these large prefactors. This is in some sense conservative, as each bond alone has many different multipolar ranks interacting. We note that the scale $\mathcal{M}$ is determined from the fitted constants $\mathcal{J}$ and thus is, in some sense, an overall scale for all the odd-rank multipolar interactions, not just those of rank 1. We thus see that assuming a classical ψ_2 selection, when the combinatoric factors are included, the rough estimate of the excitation gap increases by a factor of 100 to $\sim$0.1–1 μeV.

Furthermore, this result is sensitive to the scale of multipolar interactions between the $J = 15/2$ moments; if the scale $\mathcal{M}$ is increased by some factor, the induced gap increases by its cube, as shown in Eqs. (26) and (28). Moreover, the above estimate does not include the role played by even-rank multipolar interactions that do not contribute at first order to the scale $\mathcal{J}$ obtained from the experimental fitting. As we saw in Eq. (11), these simply give irrelevant constants when projected into the ground doublets. Given that there is no reason to expect the even-rank interactions to be smaller than the odd-rank [36,37], this could be a significant underestimate of the size of the virtual crystal field fluctuations. Beyond this, it is not *a priori* excluded that the multitude of higher odd-rank interactions could also have an effect in the virtual crystal field fluctuations that is disproportionate to their effects in the bare projection. Since our very rough estimate above is within one or two orders of magnitude or so of the $\sim$20 μeV gap estimated from quantum zero-point fluctuations [15] and the $\sim$40–45 μeV gap measured experimentally [25,26], the importance of virtual crystal fluctuations must be reevaluated. These heuristic arguments are one of the main results of this work, motivating the detailed calculations we present next. However, given the rough nature of such estimates one must be careful not to interpret them too optimistically or prematurely. In sections that follow, we confirm and expand these estimates with quantitative calculations of the energetic selection and excitation gap due to the effects of virtual crystal field fluctuations.

IV. BILINEAR-BIQUADRATIC MODEL

As argued in the previous section, simple scaling arguments suggest that the effects of virtual crystal field fluctuations could be significant in $Er_2Ti_2O_7$. To address the magnitude of these effects in a quantitative fashion, we first need an explicit model of the multipolar interactions within the $J = 15/2$ manifold, rather than the schematic form of the previous section. Determination of these multipolar interactions from experiments is a difficult endeavor; as most of the experimental data on $Er_2Ti_2O_7$ can be described almost quantitatively using the effective spin-1/2 model of Ref. [15], there are few data left to constrain the model of Eq. (6). Indeed,

only the odd-rank interactions are constrained through the projection into the effective spin-1/2 model of Eq. (2), with no constraints at all are placed on the even-rank interactions. Estimating the multipolar couplings by purely theoretical means is also similarly challenging. Given this daunting state of affairs, we will not attempt to study the full $J = 15/2$ multipolar interactions, but will restrict ourselves to some simpler caricature that captures the essential physics of having both time-reversal even and odd multipolar interactions.

The most straightforward approach [25,35] is to consider only bilinear interactions between the $J = 15/2$ moments. This takes the form

$$H_J \equiv \sum_{\langle ij \rangle} \mathbf{J}_i^{\mathsf{T}} [\boldsymbol{\lambda}^{-1} \mathcal{J}_{ij} \boldsymbol{\lambda}^{-1}] \mathbf{J}_j + \eta \sum_i \mathcal{V}(\mathbf{J}_i). \tag{29}$$

The exchanges $\boldsymbol{\lambda}^{-1} \mathcal{J}_{ij} \boldsymbol{\lambda}^{-1}$ have been chosen to reproduce Eq. (2) after one projects into the ground doublet, with $P(\boldsymbol{\lambda}^{-1} \mathbf{J}_i) P = \mathbf{S}_i$. While appealing in its simplicity, the lack of even-rank interactions or higher odd-rank interactions eliminates a possibly potent source of virtual crystal field fluctuations. To capture some aspects of these even-rank multipolar interactions that must be present in the microscopic model, we supplement this bilinear model with *biquadratic* interactions between $J = 15/2$ moments. These are couplings between rank-2 multipoles as defined in Eq. (4) with

$$H_Q \equiv \sum_{\langle ij \rangle} \sum_{QQ'} \mathcal{M}_{ij}^{2Q,2Q'} O_{2,Q}(\mathbf{J}_i) O_{2,Q'}(\mathbf{J}_j), \tag{30}$$

where $Q, Q' = 0, \pm 1, \pm 2$. The interaction matrix needs only be specified on a single bond while the rest can be determined by symmetry. While in principle unconstrained, we expect the scale of these interactions to be comparable to that of the bilinear terms. We thus consider the *bilinear-biquadratic* model

$$\begin{aligned} H \equiv H_J + \kappa H_Q + \eta H_{\mathrm{CEF}}, &= \sum_{\langle ij \rangle} \mathbf{J}_i^{\mathsf{T}} [\boldsymbol{\lambda}^{-1} \mathcal{J}_{ij} \boldsymbol{\lambda}^{-1}] \mathbf{J}_j \\ &+ \eta \sum_i \mathcal{V}(\mathbf{J}_i) + \kappa \sum_{\langle ij \rangle} \sum_{QQ'} \mathcal{M}_{ij}^{2Q,2Q'} O_{2,Q}(\mathbf{J}_i) O_{2,Q'}(\mathbf{J}_j). \end{aligned} \tag{31}$$

We have added a single tuning parameter κ, in analogy to the parameter η, to control the scale of the biquadratic interactions. To ensure we are treating the rank-1 and rank-2 interactions on equal footing, we normalize the matrix $\boldsymbol{\mathcal{M}}_{ij}^{2,2}$ so that

$$\frac{1}{5^2} \sum_{QQ'} |\mathcal{M}_{ij}^{2Q,2Q'}| = \frac{1}{3^2} \sum_{QQ'} |\mathcal{M}_{ij}^{1Q,1Q'}|, \tag{32}$$

where $\boldsymbol{\mathcal{M}}_{ij}^{11}$ are the spherical tensor components of the rank-1 interactions, as normalized in Eq. (4). In this way, the average matrix elements for the rank-1 and rank-2 interactions are equal when $\kappa = 1$.

In this model, the bilinear terms serve as a proxy for all odd-rank interactions, while the biquadratic terms do the same for all even-rank interactions. This is a drastic simplification of the multipolar interactions; the bilinear-biquadratic is a caricature of the underlying Er-Er interactions. Even with this simplification, there are a large number of free parameters. For nearest-neighbor bonds we find that there are 10 symmetry allowed independent biquadratic couplings. We will fix the ratios of these couplings using models motivated from two microscopic schemes, leaving the overall scale κ as a tuning parameter. These schemes are complementary and motivated by superexchange [14] and the microscopic electric quadrupole-quadrupole interaction [47]. We do not intend to imply that these different schemes are strictly realistic models for biquadratic exchange in $Er_2Ti_2O_7$, though both would be present in the material; they simply serve as useful parametrizations of the biquadratic couplings. Furthermore, the similarity of the results for the different biquadratic coupling schemes that we find below is a strong indication that the order by virtual crystal field fluctuation mechanism is enhanced when including any even-rank couplings, independently of the details of even-rank interactions themselves.

A. Superexchange model

One natural source of higher-multipole interactions [48] in rare-earth magnets comes from superexchange [37]. Due to the large separation of the Er^{3+} ion relative to the extent of the $4f$ orbitals, we expect that this proceeds largely through the neighboring oxygen atoms. For a detailed treatment we refer the reader to Refs. [14,39]. Here, we simply quote the form of the interaction in the so-called charging approximation [49]:

$$\sum_{\langle ij \rangle} \sum_{\alpha\beta\mu\nu} \left(P f_{i\alpha}^\dagger f_{i\beta} P \right) \mathcal{I}_{ij}^{\alpha\beta\mu\nu} \left(P f_{j\mu}^\dagger f_{j\nu} P \right), \tag{33}$$

where we have used a combined spin-orbital index $\alpha \equiv (m, \sigma)$ with $f_{i\alpha}^\dagger$ creating a $4f$ electron with spin σ and orbital m at site $\mathbf{r}_i$. The local operators can be expressed in terms of multipoles of rank K with $K \leqslant 7$:

$$P f_{i\alpha}^\dagger f_{i\beta} P \equiv \sum_{KQ} A_{KQ}^{\alpha\beta} O_{KQ}(\mathbf{J}_i), \tag{34}$$

for some set of coefficients $A_{KQ}^{\alpha\beta}$. The interaction matrix $\mathcal{I}$ is given as

$$\begin{aligned} \mathcal{I}_{ij}^{\alpha\beta\mu\nu} \equiv \frac{2}{(U_f^+ + \Delta_{fp})^2} \Bigg[&- \frac{2 [t_j t_j^\dagger]^{\mu\nu} [t_i t_i^\dagger]^{\alpha\beta}}{2U_f^+ + U_p + 2\Delta_{fp}} \\ &+ \left(\frac{1}{U_f^+ + U_f^-} + \frac{2}{2U_f^+ + U_p + 2\Delta_{fp}} \right) \\ &\times [t_j t_i^\dagger]^{\mu\beta} [t_i t_j^\dagger]^{\alpha\nu} \Bigg], \end{aligned} \tag{35}$$

where $U_f^\pm \sim E(4f^{11\pm1}) - E(4f^{11})$ gives the energy differences between adjacent charge configurations of the Er^{3+} ion. Δ_{fp} is the charge gap between the $4f$ and $2p$ levels. The t_i matrices define the $4f$-$2p$ overlap. In the Slater-Koster approximation [50], these are expressed as $t_i = R_i^\dagger t_0$ where R_i is a rotation of the f and p orbitals that takes a set of axes aligned to the local axes at site $\mathbf{r}_i$ into the global frame. The matrices t_0 define overlaps in the frame aligned along the bond axis and take the simple form $[t_0]_{mm'} = \delta_{mm'} (\delta_{|m|=1} t_{pf\pi} + \delta_{m=0} t_{pf\sigma})$.

Since $U_p > 0$ and $\Delta_{fp} > 0$, the second term in Eq. (35), with denominator $(U_f^+ + U_f^-)^{-1}$, is dominant. Taking only

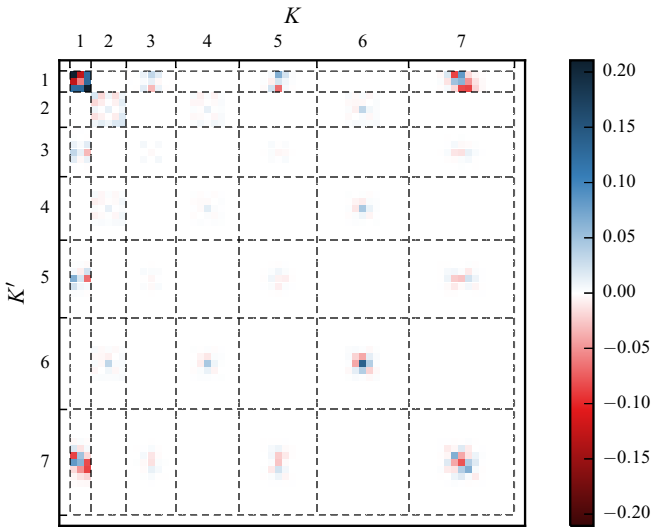

FIG. 2. Representation of the multipolar interaction matrix $\mathcal{M}$ generated by the superexchange interaction given in Eq. (35). The overall scale is arbitrary. For each pair of ranks $K, K' = 1,2,\ldots,7$ the matrix elements $\mathcal{M}^{KQK'Q'}$ can be arranged into a $2K'+1$ by $2K+1$ matrix with the Q, Q' indices running along the column and row, respectively. These blocks are shown arranged in a table by their K, K' indices, with the dashed lines showing the boundaries of each block where $Q = \pm K$ or $Q' = \pm K'$. Significant interactions beyond purely bilinear, i.e., with $K, K' > 1$, are present.

this term affords the simplification that the parameters $U_f^{\pm}$ and Δ_{pf} enter only into the overall scale of the superexchange interactions. Fixing the Slater-Koster parameters to the canonical ratio [51] $t_{pf\pi}/t_{pf\sigma} \sim -0.3$, one finds that a very complex set of multipolar interactions are generated. As illustrated in Fig. 2, these include significant odd- and even-rank interactions up to and including rank 7 [38,39]. To fit this within our bilinear-biquadratic framework, we simply truncate all multipolar interactions with rank > 2 and replace the rank-1 interactions with those of Eq. (31) to reproduce the experimentally fitted model of Eq. (2) when projected into the ground doublet. We again emphasize that this is not expected to be a quantitative model of the microscopic superexchange interactions due to the neglect of the higher multipoles as well as the charging approximation used to arrive at Eq. (35). However, we do expect this toy model to capture the essential features of even-rank interactions and thus will serve as a useful tool for exploring how these multipolar interactions affect the virtual crystal field fluctuations.

B. Electric quadrupole-quadrupole model

Another interaction between the quadrupolar degrees of freedom arises simply due to electrostatics [47,52,53]. To present this compactly, it will be useful to consider a more conventional definition of the quadrupolar operators, rather than the spherical tensor basis we have been using so far. We consider the Cartesian tensors $\mathbf{Q}_{ij}$ defined with respect to the *global* axes as

$$\mathbf{Q}_i \equiv \mathbf{R}_i^{\intercal}\left(3\overline{\mathbf{J}_i\mathbf{J}_i^{\intercal}} - J(J+1)\right)\mathbf{R}_i, \tag{36}$$

where $\mathbf{R}_i^{\intercal}\mathbf{J}_i \equiv \hat{\mathbf{x}}_i J_i^x + \hat{\mathbf{y}}_i J_i^y + \hat{\mathbf{z}}_i J_i^z$ is the moment at site $\mathbf{r}_i$ in the global axes and the product is symmetrized, i.e., $\overline{J^\mu J^\nu} \equiv (J^\mu J^\nu + J^\nu J^\mu)/2$. This is a symmetric traceless matrix with five independent components. The explicit relationship between spherical tensors defined in Eq. (4) and the Cartesian form of Eq. (36) is given Appendix D. These electric quadrupole-quadrupole (EQQ) interactions decay as $\sim 1/r^5$ so we consider only the nearest-neighbor contribution

$$\mathcal{Q}\sum_{\langle ij\rangle}\hat{\mathbf{r}}_{ij}^{\intercal}\left(\frac{1}{3}\mathrm{tr}\left[\mathbf{Q}_i\mathbf{Q}_j\right] - \frac{10}{3}\mathbf{Q}_i\mathbf{Q}_j + \frac{35}{6}\mathbf{Q}_i\hat{\mathbf{r}}_{ij}\hat{\mathbf{r}}_{ij}^{\intercal}\mathbf{Q}_j\right)\hat{\mathbf{r}}_{ij}, \tag{37}$$

where $\mathbf{r}_{ij} \equiv \mathbf{r}_i - \mathbf{r}_j$. The microscopic quadrupolar coupling constant $\mathcal{Q}$ is given by [47]

$$\mathcal{Q} \equiv \frac{\alpha_J\langle r^2\rangle^2}{r_{\mathrm{nn}}^5}\left(\frac{e^2}{4\pi\epsilon}\right) \sim 6.664\times 10^{-6}\ \mathrm{meV}. \tag{38}$$

Shielding effects likely reduce this further by a factor of $\sim$0.25 or so [47]. The smallness of this numerical value is highly misleading; given the large matrix elements $\sim J^4$ the true scale of these interactions is closer to 10^{-3} meV to 10^{-4} meV. As for the superexchange model, this interaction is used as a convenient parametric form of the biquadratic couplings and is not intended to be realistic. We thus do not use the bare microscopic interaction strength, but normalize the biquadratic couplings as given in Eq. (32), allowing the overall scale to vary via κ.

C. Mean-field and random-phase approximation

With these concrete models defined, we can now analyze the effects of the biquadratic interactions within an approach that uses mean-field theory (MFT) and the random-phase approximation (RPA) [46]. For the case of purely bilinear interactions, such an analysis has been presented in Ref. [25] (differences from the present study are discussed in Appendix C). This provides a route to estimating the gap, and thus the condensation energy, without the heavy machinery of the high-order perturbative expansion presented in Sec. II B. We lose however, the quantitative mapping to the effective spin-1/2 degrees of freedom. Still, as we shall see, the MFT and RPA results are entirely consistent with the scaling expected from the strong-coupling expansion, and even include effects that go beyond the leading order results given in Sec. II B. We formulate these methods for general multipolar interactions, then apply the results to the specific bilinear-biquadratic models discussed in Secs. IV A and IV B.

In the mean-field approximation we simply decouple the multipolar interactions as

$$O_{KQ}(\mathbf{J}_i)O_{K'Q'}(\mathbf{J}_j) \approx \mathcal{O}_j^{K'Q'}O_{KQ}(\mathbf{J}_i) + \mathcal{O}_i^{KQ}O_{K'Q'}(\mathbf{J}_j) - \mathcal{O}_i^{KQ}\mathcal{O}_j^{K'Q'}, \tag{39}$$

where $\mathcal{O}_i^{KQ} \equiv \langle O_{KQ}(\mathbf{J}_i)\rangle$ are expectation values of the multipole operators. The full multipolar exchange Hamiltonian then reduces to single-site terms

$$H \approx \sum_i\left[\eta\mathcal{V}(\mathbf{J}_i) + \sum_{KQ}h_{KQ,i}O_{KQ}(\mathbf{J}_i)\right] \equiv \sum_i\mathscr{H}_i(\mathbf{J}_i), \tag{40}$$

where we have defined the effective multipolar mean fields

$$h_{KQ,i} \equiv \sum_j \sum_{K'Q'} \left(\mathcal{M}_{ij}^{KQ,K'Q'} + \mathcal{M}_{ji}^{K'KQ'Q}\right)\mathcal{O}_j^{K'Q'}. \quad (41)$$

This defines a set of effective single-site Hamiltonians $\mathscr{H}_i$ that can be solved self-consistently for the multipole expectation values $\mathcal{O}_i^{KQ}$. This is equivalent to performing variational minimization on an ansatz that is an arbitrary product state in the $J = 15/2$ site basis.

To access the spin-wave excitation gap, Δ, we compute the dynamic susceptibility $\boldsymbol{\chi}(\mathbf{k},\omega)$ within the RPA. The imaginary part of $\boldsymbol{\chi}(\mathbf{k},\omega)$ is directly related to the intensity observed in inelastic neutron scattering experiments. With only bilinear interactions between the $\mathbf{J}_i$ moments, one can use the standard RPA equation [46]

$$[1 - \boldsymbol{\chi}^0(\omega)\boldsymbol{\mathcal{J}}(\mathbf{k})]\boldsymbol{\chi}(\mathbf{k},\omega) = \boldsymbol{\chi}^0(\omega), \quad (42)$$

where $\boldsymbol{\mathcal{J}}(\mathbf{k})$ is the Fourier transform of the bilinear exchange matrix and $\boldsymbol{\chi}^0(\omega)$ is the on-site susceptibility

$$\chi^0_{\mu\nu}(\omega) \equiv \sum_{nn'} \frac{\langle n|J_\mu|n'\rangle\langle n'|J_\nu|n\rangle}{(\omega + i0^+) - (E_{n'} - E_n)}(\rho_{n'} - \rho_n),$$

where E_n and $|n\rangle$ denote the energies and eigenstates of the single-site mean-field Hamiltonian defined in Eq. (40) and $\rho_n \equiv e^{-\beta E_n}/Z$ are the associated Boltzmann weights.

With multipolar interactions, we compute instead a generalized multipolar susceptibility $\boldsymbol{\Gamma}(\mathbf{k},\omega)$. As the derivation follows that of the conventional RPA closely [46], we simply state the final expressions. We first define the on-site, noninteracting multipolar susceptibility

$$\Gamma^0_{KQ,K'Q'}(\omega) \equiv \sum_{nn'} \frac{\langle n|O_{KQ}(\mathbf{J})|n'\rangle\langle n'|O_{K'Q'}(\mathbf{J})|n\rangle}{(\omega + i0^+) - (E_{n'} - E_n)} \times (\rho_{n'} - \rho_n). \quad (43)$$

This is can be regarded as a matrix $\boldsymbol{\Gamma}^0(\omega)$ in the basis of spherical tensors, with indices (KQ) and $(K'Q')$. The magnetic susceptibility $\boldsymbol{\chi}(\mathbf{k},\omega)$ is simply the $\Gamma_{1Q,1Q'}(\mathbf{k},\omega)$ block of $\boldsymbol{\Gamma}(\mathbf{k},\omega)$ rotated into the Cartesian basis using Eq. (5). In the RPA, the full wave-vector-dependent multipolar susceptibility $\boldsymbol{\Gamma}(\mathbf{k},\omega)$ then satisfies the equation

$$[1 - \boldsymbol{\Gamma}^0(\omega)\boldsymbol{\mathcal{M}}(\mathbf{k})]\boldsymbol{\Gamma}(\mathbf{k},\omega) = \boldsymbol{\Gamma}^0(\omega), \quad (44)$$

where $\boldsymbol{\mathcal{M}}(\mathbf{k})$ is the Fourier transform of the multipolar interaction matrix $\boldsymbol{\mathcal{M}}_{ij}$. As both $\boldsymbol{\mathcal{M}}(\mathbf{k})$ and $\boldsymbol{\Gamma}^0(\omega)$ are known, these are linear equations that can be solved for each pair $(\mathbf{k},\omega)$ to yield $\boldsymbol{\Gamma}(\mathbf{k},\omega)$. To cure the singularities, a small imaginary part is added to denominators in $\boldsymbol{\Gamma}^0(\omega)$, endowing the excitation spectrum with a slight broadening. For the bilinear-biquadratic model, Eq. (31), that we are studying, it is sufficient to consider $\boldsymbol{\Gamma}(\mathbf{k},\omega)$ as an 8×8 matrix that includes $\boldsymbol{\chi}(\mathbf{k},\omega)$, a 5×5 quadrupolar susceptibility, as well as off-diagonal bilinear-biquadratic mixing terms.

V. RESULTS

The MFT is formulated in terms of the order parameters for rank-1 and rank-2 multipoles, defined as

$$\mathbf{m}_i \equiv \langle \mathbf{J}_i \rangle, \quad q_{Q,i} \equiv \langle O_{2,Q}(\mathbf{J}_i)\rangle. \quad (45)$$

The five expectation values $q_{Q,i}$ can be organized as a vector $\mathbf{q}_i \equiv (q_{+2,i}\ \ q_{+1,i}\ \ q_{0,i}\ \ q_{-1,i}\ \ q_{-2,i})$. We note that the $q_{0,i}$ component is nonzero even without any ordering as $O_{2,0}(\mathbf{J}_i)$ breaks no symmetries of the model. Concretely, this is due to the presence of the crystalline electric field. Solving the self-consistent equations with both $\mathbf{m}$ and $\mathbf{q}$ allowed to vary within the tetrahedral unit cell, we generically find a ψ_2 state with uniform mean fields $\mathbf{m}_i \equiv \mathbf{m}$ and $\mathbf{q}_i \equiv \mathbf{q}$. In contrast to the effective spin-1/2 model of Eq. (2), the degeneracy of the Γ_5 manifold is already lifted at the mean-field level through the inclusion of the higher crystal field levels, as previously found in Refs. [25,35]. In this local basis, the ψ_2 states are characterized by the expectation value $\mathbf{m}$, taking one of the six symmetry related solutions

$$\mathbf{m} = \pm m_\perp \hat{\mathbf{x}} \mp m_z \hat{\mathbf{z}} \quad (46a)$$

$$= \pm m_\perp \left(-\frac{1}{2}\hat{\mathbf{x}} \pm \frac{\sqrt{3}}{2}\hat{\mathbf{y}}\right) \mp m_z \hat{\mathbf{z}} \quad (46b)$$

$$= \pm m_\perp \left(-\frac{1}{2}\hat{\mathbf{x}} \mp \frac{\sqrt{3}}{2}\hat{\mathbf{y}}\right) \mp m_z \hat{\mathbf{z}}, \quad (46c)$$

with $m_\perp \sim O(1)$ and $|m_z| \ll m_\perp$ at low temperature. One can think of these as planar ψ_2 states with a small amount of canting into the local $\hat{\mathbf{z}}$ direction, as expected from the analysis of Sec. III A. The small component m_z is a secondary order parameter and is pinned as $m_z \propto m_\perp^3$ as temperature is varied. This can be understood at the level of Landau-Ginzburg theory where allowed terms such $\sim m_z m_\perp^3$ cause $m_\perp^3$ to act as a conjugate field to m_z in the ordered phase [29]. As m_z is induced by the four-spin term C_4, it gives some indication of the magnitudes of energetic selection and excitation gap. However, as we saw in Sec. III A, both these effects depend not only on C_4 but on the six-spin term C_6 as well. Since the small $m_z \sim \theta_0$ moment is independent of C_6 [see Eq. (22)], the magnitude of $|m_z|$ gives only a partial picture of the selection mechanism. This is particularly true in regions where m_z, and thus C_4, change sign relative to $m_\perp$.

The exact values of $m_\perp$ and m_z depend on the crystal field and exchange parameter sets used as well as the strength of the biquadratic coupling. For definiteness, we focus on the crystal field parametrization of Bertin *et al.* [22] with the bilinear exchange parameters of Savary *et al.* [15] (see Appendix B) mapped to bilinear interactions as in Eq. (29). Results using other parameter sets (see Appendix B) from the literature give qualitatively similar values. We then can gain some insight into the effects of the biquadratic interactions by looking at the dependence of $|m_z|$ on the tuning parameter κ at $T = 0$. We present these results for the superexchange and EQQ model interactions in Fig. 3. For $\kappa = 0$ one find that $|m_z|$ is small but finite, of order $\sim 10^{-2}$. This is purely a consequence of the high-lying crystal field states, as can be seen by looking at the dependence of $|m_z|$ on the crystal field rescaling η. As shown in Fig. 3, it scales as $\sim \eta^{-2}$ as expected from Sec. III A. Turning to the effect of finite κ, we see that the magnitude of m_z increases dramatically from the bare value $|m_z| \sim 10^{-2}$ present at $\kappa = 0$. This indicates generation of a four-spin term and thus that the selection of the ψ_2 state can be significantly enhanced by

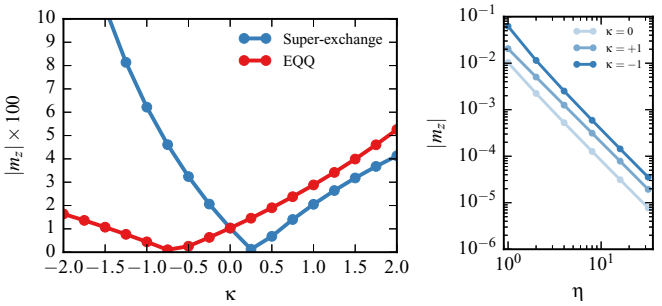

FIG. 3. (a) Dependence of the canted moment m_z on the biquadratic coupling strength κ in the superexchange and EQQ cases. Note that throughout the range $|m_z|$ is at most ∼0.1 while the in-plane components $m_\perp$ take on a value ∼3 expected from the effective-spin picture. (b) Dependence of $|m_z|$ on the crystal field rescaling η, showing the η^{-2} scaling for several values of κ for the superexchange model.

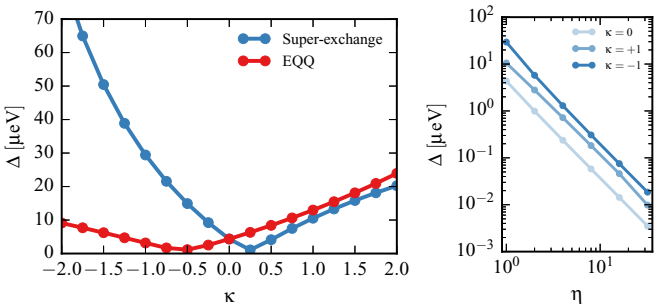

FIG. 4. (a) Dependence of the excitation gap Δ on the biquadratic coupling strength κ for superexchange and EQQ type interactions. Note that for $\kappa \sim 2$ both superexchange and EQQ give a gap of ∼20 μeV, comparable to that found for order by quantum disorder. For the superexchange model with $\kappa \sim -1.5$, the gap approaches the experimental value of ∼40–45 μeV. (b) Dependence of Δ on the crystal field rescaling η, showing the η^{-2} scaling for several values of κ for the superexchange model.

including biquadratic interactions, or more generally, high-rank multipolar interactions.

Experimentally, while the selection itself can be observed [20,23], there is no good way to probe the condensation energy, δE, directly. Instead, we look to the gap in the excitation spectrum via the RPA. As to more closely compare with the experimental results, we present the dynamic structure factor as would be seen in inelastic neutron scattering experiments [46]

$$S(\mathbf{k},\omega) \propto \sum_{\mu\nu} \left(\delta_{\mu\nu} - \frac{k^\mu k^\nu}{|\mathbf{k}|^2}\right) \frac{\mathrm{Im}\chi^{\mu\nu}(\mathbf{k},\omega)}{1 - e^{-\beta\omega}}, \qquad (47)$$

which is directly related to the results of inelastic neutron scattering experiments [15,31]. We average over the six domains of the ψ_2 ordering, as given in Eq. (46), to compare directly with experimental results. For simplicity, we do not include the magnetic form factor of Er^{3+}. The gap size as a function of κ is shown in Fig. 4. As in the case of m_z, the scaling of the gap with the crystal field is also consistent with the order by virtual crystal field fluctuations scenario; the gap closes as η^{-2}, as expected from Sec. III A. The minima as a function of κ are those points where m_z, and thus C_4, change sign relative to $m_\perp$, and selection is purely from C_6. As shown in Fig. 4, the excitation gap is strongly dependent on the strength of the biquadratic coupling; for moderate but reasonable values of κ, one can find a gap that is comparable to or larger than that found in the order by quantum disorder scenario [15]. In fact, when the biquadratic coupling is comparable to the bilinear coupling, this gap can easily be made consistent with experimental estimates. For the superexchange model, this occurs near $\kappa \sim -1.5$, while for the EQQ model this is at the larger value $\kappa \sim 3.5$. Note that the gross features of the excitation spectrum are preserved when a finite biquadratic coupling is introduced. For concreteness, we compare the $\eta \to \infty$ limit where our model reduces to an effective spin-1/2 model as shown in Fig. 5 to the result with finite superexchange type biquadratic interactions shown in Fig. 6. The biquadratic coupling has been chosen to be $\kappa = -1.5$ to reproduce the experimental gap size. Aside from the gap at [111] and small upward shift in energy, the features of the two spectra are nearly indistinguishable. Comparing to the experimental results of Ref. [15] or Ref. [25] we find that, aside from the gap, the model with the biquadratic coupling fits the data as well as the effective spin-1/2 model within theoretical and experimental uncertainties. This agreement should be further improved by renormalizing the bare $\mathcal{J}$ couplings to remove the second-order shifts from virtual crystal field fluctuations. This qualitative similarity persists past the point $\kappa = 1$, where we consider the bilinear and biquadratic interactions to be of comparable magnitude. Indeed, we can extend the EQQ model to the larger value $\kappa \sim 3.5$ and still obtain a spectrum nearly identical to that shown in Fig. 6. This indicates that there is a wide range of biquadratic coupling strengths that induce a significant gap and remain consistent with the overall features of the excitation spectrum as reported in Ref. [15].

These two consequences of the biquadratic interactions, the large induced gap and the invariance of the broad features of the spectrum, form the main result of this work. Together, they imply that significant biquadratic coupling can not only produce a gap large enough to account for the observed results but, crucially, can do so without spoiling the agreement between the excitation spectrum and experiments. More generally, this tells us that the higher multipolar interactions, which are expected to be not only present but significant [37], can have observable effects at low energies. With this proof of principle, we see that virtual crystal field effects cannot necessarily be ignored. Next we discuss how this scenario could be tested in $Er_2Ti_2O_7$.

VI. DISCUSSION

The question of the role of order by disorder mechanism in $Er_2Ti_2O_7$ is a quantitative, not a qualitative question. Given any mechanism that selects the ψ_2 state from the Γ_5 manifold, one expects a soft mode in the spin-wave spectrum with a small gap [30]. Thus the observed excitation gap is a consequence of the ψ_2 selection and does not provide a signature for any given selection mechanism. The identification of the mechanism thus lies in the details, for example through the absolute magnitude

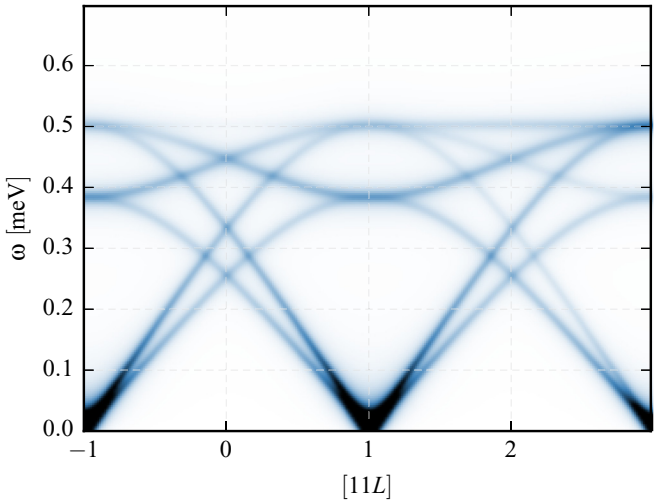

FIG. 5. Excitation spectrum of the effective spin-1/2 model ($\eta \to \infty$) in the RPA, cut along the [11L] direction. Intensity scale is arbitrary. The gapless mode is visible near [111].

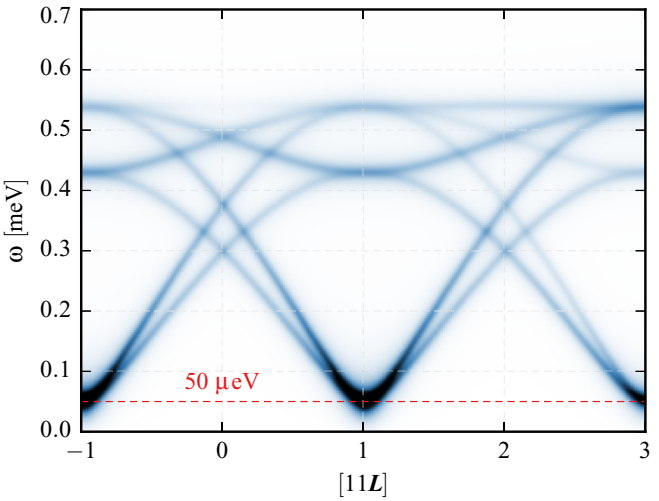

FIG. 6. Excitation spectrum of the bilinear-biquadratic model ($\eta = 1$) in the RPA, shown for superexchange interactions with $\kappa = -1.5$ along the [11L] direction. Intensity scale is arbitrary. Aside from the ∼50 μeV gap near [111], the bands show a very strong similarity to the spin-1/2 case ($\eta \to \infty$) in Fig. 5.

of the gap or dependence on other effects such as random disorder or magnetic field. In the order by quantum disorder order scenario of Ref. [15], this final identification rested on the effects of virtual crystal field fluctuations being taken to be entirely negligible. As established in Secs. III, IV, and V, the assumptions unpinning this conclusion are unwarranted. Not only are the effects of virtual crystal field fluctuations non-negligible; they can be comparable to or even larger than the corresponding quantum fluctuations when multipolar interactions are taken into account. We are thus left with the difficult task of disentangling these two fluctuation effects, as both will be present generically.

We first should focus on the magnitude of the gap seen experimentally. In Refs. [25,26] a gap of ∼40–45 μeV is observed. In the order by quantum disorder scenario, the excitation gap is fully determined from the fitted exchanges of the effective spin-1/2 model. However, this model is not analytically or numerically tractable; given these theoretical limitations we must resort to approximate methods to estimate the gap. In Ref. [15], the large-S result from linear spin-wave theory (LSWT) is extrapolated to $S = 1/2$ giving a gap of $\Delta \sim 20$ μeV, about 50% of the observed gap size. A complementary perturbative approach undertaken in Ref. [33] suggests that effects beyond LSWT could further reduce this value. Using real-space perturbation theory, Ref. [33] finds that the $U(1)$ breaking term obtained from LSWT is exactly canceled at higher order in perturbation theory when evaluated for $S = 1/2$. A more careful calculation [33] gives a degeneracy lifting δE that is reduced by ∼40% from the value reported in Ref. [15]. Since we expect $\Delta^2 \sim C_2 \delta E$ [see Eq. (27)], this would reduce the gap size and move us significantly further away from the experimental result. If taken at face value, these estimates suggest that the order by quantum disorder contribution to the condensation energy of the ψ_2 state could be as little as 25% of the value inferred from the experimental gap. This raises some doubt to whether order by quantum disorder is the leading origin of ψ_2 selection in $Er_2Ti_2O_7$.

Another indirect probe into the selection mechanism is provided by the effects of disorder. It has been argued [33,34] that diluting Er^{3+} in $Er_2Ti_2O_7$ with nonmagnetic Y^{3+} ions could provide another mechanism to break the degeneracy of the Γ_5 manifold. Such dilution favors the ψ_3 state, not the ψ_2 state found in the clean limit. This presents the intriguing possibility that by a controlled introduction of vacancies at the Er^{3+} sites, one could tune from the ψ_2 state into the ψ_3 state. The critical dilution would provide some indication of condensation energy that stabilizes the ψ_2 state. Estimating this critical dilution, ρ_c, suffers from many of the theoretical limitations such as estimating the gap in the pure effective spin-1/2 model. In Ref. [33], this is estimated to be as low as $\rho_c \sim 7\%$, taking the degeneracy lifting term δE to be ∼40% of the LSWT result, as described above. If instead of relying on the theoretical stabilization energy, we extract δE from the *experimental* gap using Eq. (27), one obtains a δE that is four times larger. An equivalent enhancement of ρ_c follows, raising the critical dilution to 25% or so. This could provide further evidence towards a stronger selection effect than predicted by the order by quantum disorder proposals.

The question then remains: what is responsible for the remaining stabilization of the ψ_2 state? The results presented here suggest that this quantitative difference could be resolved through the effects of virtual crystal field fluctuations. Further, we have shown that the full experimental gap can be accounted for with reasonable values of the biquadratic coupling. Accounting for only the fraction remaining after order by quantum disorder requires even less biquadratic coupling. We caution that a definitive experimental signature of this order by virtual crystal field fluctuations mechanism is difficult to formulate. These questions are highly quantitative and, given the small scale of these effects, are thus muddled by the combination of theoretical and experimental uncertainties. In principle, the presence of higher-rank multipolar couplings could be probed by looking at the dispersion of the higher crystal field levels in the ordered state. For example, a rough

estimate of the magnitude of the higher multipolar interactions could be inferred by comparing with predictions assuming only the bilinear interactions of Eq. (29). However, given the large number of independent parameters defining the multipolar couplings, extracting a definite scale for the higher-rank parts is likely to be an ill-posed challenge. Another possible signature could be the finite m_z moment. Indeed, this is zero at leading order in the LSWT of Ref. [15] and in the real-space perturbation theory of Ref. [33]. There are several difficulties with this: it is generically expected to be finite for the ψ_2 state, as it is allowed by symmetry [29], and thus should appear at higher order in both such theories. Further, the relationship between the size of m_z and the condensation energy is indirect, and even when enhanced it may be too small to be observed experimentally.

VII. CONCLUSION

The concept of order by disorder is a cornerstone of the theory of highly frustrated magnetism [3,4,7], representing a middle ground between ordering in an unfrustrated system and a fully magnetically disordered state. However, due to the need for a nearly accidental symmetry and the difficulty in distinguishing it from more conventional ordering scenario, clear material examples are scarce. Even in a compelling material such as $Er_2Ti_2O_7$, we have shown here that it is difficult to distinguish between possible selection mechanisms. But not all interesting physics is lost; we have proposed an order by disorder mechanism that proceeds through the virtual crystal field excitations of the Er^{3+} ion. Despite the naively large crystal field energy scale, this order by virtual crystal field fluctuations can be quite effective in selecting the ordered ground state. While the selection induced solely by bilinear interactions is to some extent weaker than that seen experimentally (e.g., the gap, Δ, is roughly five times too small), once multipolar interactions are taken into account, we find this mechanism to be competitive with order by quantum disorder and is able to account for the experimentally observed excitation gap, maintaining agreement with the rest of the excitation spectrum. While determining the relative size of the contributions of each of these mechanism is difficult, the availability of high-quality single crystals of $Er_2Ti_2O_7$ provides some hope that these effects could ultimately be disentangled. We further note that this selection mechanism is generically present in rare-earth magnets, with its relevance primarily controlled by the gap to the excited crystal field states.

To obtain a clearer signal for order by quantum or thermal disorder, one should then look for materials with a larger crystal field scale. A good candidate may be provided by $Yb_2Ge_2O_7$ [54] which should be described using the same effective spin-1/2 model as $Er_2Ti_2O_7$ at low energies [55,56]. As the related material $Yb_2Ti_2O_7$ appears to be proximate to the Γ_5 phase [55,56], it is plausible [54] that the ground state of $Yb_2Ge_2O_7$ is drawn from this manifold though a direct measurement is lacking. All of the considerations for $Er_2Ti_2O_7$ are then applicable, with the significant difference that the crystal field energy scale in $Yb_2Ge_2O_7$, as in $Yb_2Ti_2O_7$ [22], is likely an order of magnitude larger. This renders the order by virtual crystal field fluctuations mechanism described in the present work negligible, leaving for all practical purposes only quantum fluctuations to select the ground state.

Note added in proof. Recently, Ref. [58] has appeared showing that $Yb_2Ge_2O_7$ indeed has a Γ_5 ground state.

ACKNOWLEDGMENTS

This work was supported by the NSERC of Canada, the Canada Research Chair program (M.G., Tier 1), the Canadian Foundation for Advanced Research, and the Perimeter Institute (PI) for Theoretical Physics. Research at PI is supported by the Government of Canada through Industry Canada and by the Province of Ontario through the Ministry of Economic Development & Innovation. M.G. acknowledges the hospitality and generous support of the Quantum Matter Institute at the University of British Columbia and TRIUMF where part of this work was completed.

APPENDIX A: LOCAL BASIS

We follow the conventions of Savary *et al.* [15] and work in the basis local to each pyrochlore site. From the global basis, these local axes are defined as

$$\begin{aligned}
\hat{\mathbf{z}}_1 &= \frac{1}{\sqrt{3}}(+\hat{\mathbf{x}}+\hat{\mathbf{y}}+\hat{\mathbf{z}}), \quad \hat{\mathbf{x}}_1 = \frac{1}{\sqrt{6}}(-2\hat{\mathbf{x}}+\hat{\mathbf{y}}+\hat{\mathbf{z}}),\\
\hat{\mathbf{z}}_2 &= \frac{1}{\sqrt{3}}(+\hat{\mathbf{x}}-\hat{\mathbf{y}}-\hat{\mathbf{z}}), \quad \hat{\mathbf{x}}_2 = \frac{1}{\sqrt{6}}(-2\hat{\mathbf{x}}-\hat{\mathbf{y}}-\hat{\mathbf{z}}),\\
\hat{\mathbf{z}}_3 &= \frac{1}{\sqrt{3}}(-\hat{\mathbf{x}}+\hat{\mathbf{y}}-\hat{\mathbf{z}}), \quad \hat{\mathbf{x}}_3 = \frac{1}{\sqrt{6}}(+2\hat{\mathbf{x}}+\hat{\mathbf{y}}-\hat{\mathbf{z}}),\\
\hat{\mathbf{z}}_4 &= \frac{1}{\sqrt{3}}(-\hat{\mathbf{x}}-\hat{\mathbf{y}}+\hat{\mathbf{z}}), \quad \hat{\mathbf{x}}_4 = \frac{1}{\sqrt{6}}(+2\hat{\mathbf{x}}-\hat{\mathbf{y}}+\hat{\mathbf{z}}),
\end{aligned} \tag{A1}$$

where $\hat{\mathbf{y}}_i = \hat{\mathbf{z}}_i \times \hat{\mathbf{x}}_i$. The bond phase factors γ_{ij} and $\zeta_{ij} = -\gamma_{ij}^*$ depend only on the basis sites they connect and thus can be expressed as a matrix

$$\gamma = \begin{pmatrix} 0 & +1 & \omega & \omega^2 \\ +1 & 0 & \omega^2 & \omega \\ \omega & \omega^2 & 0 & +1 \\ \omega^2 & \omega & +1 & 0 \end{pmatrix}, \tag{A2}$$

where $\omega = e^{2\pi i/3}$.

APPENDIX B: MODEL PARAMETERS

1. Crystal fields

Several parametrizations of the crystal field potential for the Er^{3+} ion in $Er_2Ti_2O_7$ exist. We consider two of these parameter sets: those of Petit *et al.* [25] and Bertin *et al.* [22]. Both provide a good description of the crystal field levels observed experimentally. Considering the results for these two parameters sets serves as a benchmark to the sensitivity of our conclusions to the precise details of the crystal field potential. We write the crystal field potential $\mathcal{V}(\mathbf{J})$ as

$$\mathcal{V}(\mathbf{J}) = \sum_{KQ} B_{KQ}\tilde{O}_{KQ}(\mathbf{J}), \tag{B1}$$

where the $\tilde{O}_{KQ}(\mathbf{J})$ are Stevens operators [41] defined using the conventions listed in Jensen and Mackintosh [46]. Converted into the Stevens convention, the nonzero parameters of Petit

et al. [25] are

$$B_{20} = +6.741 \times 10^{-2}\ \text{meV}, \quad B_{40} = +1.363 \times 10^{-3}\ \text{meV},$$
$$B_{43} = -8.998 \times 10^{-3}\ \text{meV}, \quad B_{60} = +9.565 \times 10^{-6}\ \text{meV},$$
$$B_{63} = +1.113 \times 10^{-4}\ \text{meV}, \quad B_{66} = +1.661 \times 10^{-4}\ \text{meV}. \tag{B2}$$

The ground state λ factors are given by $\lambda_\pm = 5.706$ and $\lambda_z = 2.136$ and the first excited doublet lies at 7.51 meV. The parameters of Bertin *et al.* [22] are given by

$$B_{20} = +7.50 \times 10^{-2}\ \text{meV}, \quad B_{40} = +1.41 \times 10^{-3}\ \text{meV},$$
$$B_{43} = +1.25 \times 10^{-2}\ \text{meV}, \quad B_{60} = +1.09 \times 10^{-5}\ \text{meV},$$
$$B_{63} = -1.80 \times 10^{-4}\ \text{meV}, \quad B_{66} = +1.50 \times 10^{-4}\ \text{meV}. \tag{B3}$$

The ground state λ factors are given by $\lambda_\pm = 6.434$ and $\lambda_z = 1.758$ and the first excited doublet lies at 6.15 meV.

2. Exchanges

Estimates for the exchanges in the effective spin-1/2 model have been extracted from fitting the excitation spectrum seen in inelastic neutron scattering experiments [15,25]. The fitting of Savary *et al.* [15] was done in a magnetic field and yields the parameters

$$\mathcal{J}_{zz} = -2.50 \pm 1.80 \times 10^{-2}\ \text{meV},$$
$$\mathcal{J}_{\pm} = +6.50 \pm 0.75 \times 10^{-2}\ \text{meV},$$
$$\mathcal{J}_{\pm\pm} = +4.20 \pm 0.50 \times 10^{-2}\ \text{meV},$$
$$\mathcal{J}_{z\pm} = -0.88 \pm 1.50 \times 10^{-2}\ \text{meV}. \tag{B4}$$

The fitting of Petit *et al.* [25] was done in zero-field and yields (model B)

$$\mathcal{J}_{zz} = -2.2 \pm 0.1 \times 10^{-2}\ \text{meV},$$
$$\mathcal{J}_{\pm} = +6.0 \pm 0.1 \times 10^{-2}\ \text{meV},$$
$$\mathcal{J}_{\pm\pm} = +4.3 \pm 0.1 \times 10^{-2}\ \text{meV},$$
$$\mathcal{J}_{z\pm} = -1.5 \pm 0.1 \times 10^{-2}\ \text{meV}. \tag{B5}$$

Petit *et al.* [25] also did a fit directly using an RPA calculation within the full $J = 15/2$ manifold. Projected into the effective spin-1/2 model this yields (model A)

$$\mathcal{J}_{zz} = -0.84 \pm 0.1 \times 10^{-2}\ \text{meV},$$
$$\mathcal{J}_{\pm} = +5.93 \pm 0.1 \times 10^{-2}\ \text{meV},$$
$$\mathcal{J}_{\pm\pm} = +4.61 \pm 0.1 \times 10^{-2}\ \text{meV},$$
$$\mathcal{J}_{z\pm} = +0.91 \pm 0.1 \times 10^{-2}\ \text{meV}. \tag{B6}$$

These three parameter sets are qualitatively compatible: each has large positive in-plane exchanges $\mathcal{J}_\pm$ and $\mathcal{J}_{\pm\pm}$ with smaller $\mathcal{J}_{zz}$ and $\mathcal{J}_{z\pm}$ couplings.

APPENDIX C: DIFFERENCES FROM PETIT *ET AL.* [25]

In Petit *et al.* [25], a theoretical gap size of $\sim 15\ \mu$eV was reported, with an $\eta^{-1/2}$ dependence under crystal field rescaling. This was computed through the same RPA approximation discussed in Sec. IV C, but using a model that has only bilinear interactions between the **J** moments. These results were computed using a cutoff in the computation of the RPA excitation spectrum; some of the highest lying crystal field states were omitted from the calculation. This has significant effects on the $\eta \to \infty$ limit, effectively removing the $U(1)$ degeneracy that should appear in the effective spin-1/2 model. This causes the erroneously large gap size and the incorrect $\eta^{-1/2}$ scaling reported in Petit *et al.* [25].

APPENDIX D: SPHERICAL VERSUS CARTESIAN QUADRUPOLES

Here we give the relationship between the Cartesian quadrupoles of Eq. (36) and the spherical tensors defined in Eq. (4):

$$O_{2,0}(\mathbf{J}) = \frac{1}{12\sqrt{357}} Q^{zz}, \tag{D1a}$$

$$O_{2,\pm1}(\mathbf{J}) = \pm\frac{1}{12\sqrt{357}}\left[\sqrt{\frac{2}{3}}\left(Q^{xz} \pm i\,Q^{yz}\right)\right], \tag{D1b}$$

$$O_{2,\pm2}(\mathbf{J}) = \frac{1}{12\sqrt{357}}\left[\sqrt{\frac{1}{6}}\left(Q^{xx} - Q^{yy} \pm 2i\,Q^{xy}\right)\right]. \tag{D1c}$$

[1] Claudine Lacroix, Philippe Mendels, and Frédéric Mila, editors, *Introduction to Frustrated Magnetism* (Springer, Berlin, 2011).

[2] L. Balents, Spin liquids in frustrated magnets, Nature (London) **464**, 199 (2010).

[3] M. J. P. Gingras and P. A. McClarty, Quantum spin ice: A search for gapless quantum spin liquids in pyrochlore magnets, Rep. Prog. Phys. **77**, 056501 (2014).

[4] J. Villain, R. Bidaux, J.-P. Carton, and R. Conte, Order as an effect of disorder, J. Phys. **41**, 1263 (1980).

[5] E. F. Shender, Antiferromagnetic garnets with fluctuationally interacting sublattices, Zh. Eksp. Teor. Fiz. **83**, 326 (1982) [Sov. Phys. JETP **56**, 178 (1982)].

[6] S. Coleman and E. Weinberg, Radiative corrections as the origin of spontaneous symmetry breaking, Phys. Rev. D **7**, 1888 (1973).

[7] C. L. Henley, Ordering Due to Disorder in a Frustrated Vector Antiferromagnet, Phys. Rev. Lett. **62**, 2056 (1989).

[8] A. Chubukov, Order from Disorder in a Kagome Antiferromagnet, Phys. Rev. Lett. **69**, 832 (1992).

[9] J. R. Tessman, Magnetic anisotropy at 0° K, Phys. Rev. **96**, 1192 (1954).

[10] J. H. van Vleck, On the anisotropy of cubic ferromagnetic crystals, Phys. Rev. **52**, 1178 (1937).

[11] C. Kittel, Dipolar domains in paramagnetic crystals at low temperatures, Phys. Rev. **82**, 965 (1951).

[12] J. S. Gardner, M. J. P. Gingras, and J. E. Greedan, Magnetic pyrochlore oxides, Rev. Mod. Phys. **82**, 53 (2010).

[13] K. A. Ross, L. Savary, B. D. Gaulin, and L. Balents, Quantum Excitations in Quantum Spin Ice, Phys. Rev. X **1**, 021002 (2011).

[14] S. Onoda and Y. Tanaka, Quantum fluctuations in the effective pseudospin-1/2 model for magnetic pyrochlore oxides, Phys. Rev. B **83**, 094411 (2011).

[15] L. Savary, K. A. Ross, B. D. Gaulin, J. P. C. Ruff, and L. Balents, Order by Quantum Disorder in $Er_2Ti_2O_7$, Phys. Rev. Lett. **109**, 167201 (2012).

[16] S. H. Curnoe, Quantum spin configurations in $Tb_2Ti_2O_7$, Phys. Rev. B **75**, 212404 (2007).

[17] Han Yan, Owen Benton, Ludovic D. C. Jaubert, and Nic Shannon, Living on the edge: Ground-state selection in quantum spin-ice pyrochlores, arXiv:1311.3501.

[18] Lucile Savary and Leon Balents, Spin liquid regimes at nonzero temperature in quantum spin ice, Phys. Rev. B **87**, 205130 (2013).

[19] A. W. C. Wong, Z. Hao, and M. J. P. Gingras, Ground state phase diagram of generic XY pyrochlore magnets with quantum fluctuations, Phys. Rev. B **88**, 144402 (2013).

[20] J. D. M. Champion, M. J. Harris, P. C. W. Holdsworth, A. S. Wills, G. Balakrishnan, S. T. Bramwell, E. Čižmár, T. Fennell, J. S. Gardner, J. Lago, D. F. McMorrow, M. Orendáč, A. Orendáčová, D. McK. Paul, R. I. Smith, M. T. F. Telling, and A. Wildes, $Er_2Ti_2O_7$: Evidence of quantum order by disorder in a frustrated antiferromagnet, Phys. Rev. B **68**, 020401(R) (2003).

[21] B. Z. Malkin, T. T. A. Lummen, P. H. M. van Loosdrecht, G. Dhalenne, and A. R. Zakirov, Static magnetic susceptibility, crystal field and exchange interactions in rare earth titanate pyrochlores, J. Phys.: Condens. Matter **22**, 276003 (2010).

[22] A. Bertin, Y. Chapuis, P. Dalmas de Réotier, and A. Yaouanc, Crystal electric field in the $R_2Ti_2O_7$ pyrochlore compounds, J. Phys.: Condens. Matter **24**, 256003 (2012).

[23] A. Poole, A. S. Wills, and E. Lelièvre-Berna, Magnetic ordering in the XY pyrochlore antiferromagnet $Er_2Ti_2O_7$: A spherical neutron polarimetry study, J. Phys.: Condens. Matter **19**, 452201 (2007).

[24] J. P. C. Ruff, J. P. Clancy, A. Bourque, M. A. White, M. Ramazanoglu, J. S. Gardner, Y. Qiu, J. R. D. Copley, M. B. Johnson, H. A. Dabkowska, and B. D. Gaulin, Spin Waves and Quantum Criticality in the Frustrated XY Pyrochlore Antiferromagnet $Er_2Ti_2O_7$, Phys. Rev. Lett. **101**, 147205 (2008).

[25] S. Petit, J. Robert, S. Guitteny, P. Bonville, C. Decorse, J. Ollivier, H. Mutka, M. J. P. Gingras, and I. Mirebeau, Order by disorder or energetic selection of the ground state in the XY pyrochlore antiferromagnet $Er_2Ti_2O_7$: An inelastic neutron scattering study, Phys. Rev. B **90**, 060410 (2014).

[26] K. A. Ross, Y. Qiu, J. R. D. Copley, H. A. Dabkowska, and B. D. Gaulin, Order by Disorder Spin Wave Gap in the XY Pyrochlore Magnet $Er_2Ti_2O_7$, Phys. Rev. Lett. **112**, 057201 (2014).

[27] K. Baroudi, B. D. Gaulin, S. H. Lapidus, J. Gaudet, and R. J. Cava, Symmetry and light stuffing of $Ho_2Ti_2O_7$, $Er_2Ti_2O_7$, and $Yb_2Ti_2O_7$ characterized by synchrotron x-ray diffraction, Phys. Rev. B **92**, 024110 (2015).

[28] J. Oitmaa, R. R. P. Singh, B. Javanparast, A. G. R. Day, B. V. Bagheri, and M. J. P. Gingras, Phase transition and thermal order-by-disorder in the pyrochlore antiferromagnet $Er_2Ti_2O_7$: A high-temperature series expansion study, Phys. Rev. B **88**, 220404 (2013).

[29] B. Javanparast, A. G. R. Day, Z. Hao, and M. J. P. Gingras, Order-by-disorder near criticality in XY pyrochlore magnets, Phys. Rev. B **91**, 174424 (2015).

[30] P. A. McClarty, P. Stasiak, and M. J. P. Gingras, Order-by-disorder in the XY pyrochlore antiferromagnet, Phys. Rev. B **89**, 024425 (2014).

[31] M. E. Zhitomirsky, M. V. Gvozdikova, P. C. W. Holdsworth, and R. Moessner, Quantum Order by Disorder and Accidental Soft Mode in $Er_2Ti_2O_7$, Phys. Rev. Lett. **109**, 077204 (2012).

[32] M. E. Zhitomirsky, P. C. W. Holdsworth, and R. Moessner, Nature of finite-temperature transition in anisotropic pyrochlore $Er_2Ti_2O_7$, Phys. Rev. B **89**, 140403 (2014).

[33] V. S. Maryasin and M. E. Zhitomirsky, Order from structural disorder in the XY pyrochlore antiferromagnet $Er_2Ti_2O_7$, Phys. Rev. B **90**, 094412 (2014).

[34] A. Andreanov and P. A. McClarty, Order induced by dilution in pyrochlore XY antiferromagnets, Phys. Rev. B **91**, 064401 (2015).

[35] P. A. McClarty, S. H. Curnoe, and M. J. P. Gingras, Energetic selection of ordered states in a model of the $Er_2Ti_2O_7$ frustrated pyrochlore XY antiferromagnet, J. Phys.: Conf. Ser. **145**, 012032 (2009).

[36] R. J. Elliott, Orbital effects on exchange interactions, J. Appl. Phys. **39**, 802 (1968).

[37] P. Santini, S. Carretta, G. Amoretti, R. Caciuffo, N. Magnani, and G. H. Lander, Multipolar interactions in f-electron systems: The paradigm of actinide dioxides, Rev. Mod. Phys. **81**, 807 (2009).

[38] N. Iwahara and L. F. Chibotaru, Exchange interaction between J multiplets, Phys. Rev. B **91**, 174438 (2015).

[39] J. G. Rau and M. J. P. Gingras, How quantum are classical spin ices? Phys. Rev. B **92**, 144417 (2015).

[40] Y.-P. Huang, G. Chen, and M. Hermele, Quantum Spin Ices and Topological Phases from Dipolar-Octupolar Doublets on the Pyrochlore Lattice, Phys. Rev. Lett. **112**, 167203 (2014).

[41] K. W. H. Stevens, Matrix elements and operator equivalents connected with the magnetic properties of rare earth ions, Proc. Phys. Soc. A **65**, 209 (1952).

[42] I. Lindgren, The Rayleigh-Schrödinger perturbation and the linked-diagram theorem for a multi-configurational model space, J. Phys. B: At. Mol. Phys. **7**, 2441 (1974).

[43] The higher order terms $H_{\mathrm{eff},3}$ and $H_{\mathrm{eff},5}$ have been symmetrized via $H_{\mathrm{eff,n}} \to (H_{\mathrm{eff,n}} + H_{\mathrm{eff,n}}{}^{\dagger})/2$ to render the effective Hamiltonian Hermitian. This procedure can be justified in that there exists a transformation that maps the unsymmetrized form into the symmetrized form, as discussed by [57].

[44] H. R. Molavian, M. J. P. Gingras, and B. Canals, Dynamically Induced Frustration as a Route to a Quantum Spin Ice State in $Tb_2Ti_2O_7$ via Virtual Crystal Field Excitations and Quantum Many-Body Effects, Phys. Rev. Lett. **98**, 157204 (2007).

[45] We note that contributions to the energy such as $\cos(6n\phi)$ are also allowed. Since each of these terms carries a factor S^{6n}, for $S = 1/2$ we will neglect all but the $n = 1$ case which has been considered.

[46] J. Jensen and A. R. Mackintosh, *Rare Earth Magnetism* (Clarendon, Oxford, 1991).

[47] W. P. Wolf and R. J. Birgeneau, Electric multipole interactions between rare-earth ions, Phys. Rev. **166**, 376 (1968).

[48] Note that due to the large orbital moments in the Er^{3+} ground doublets, superexchange generates multipolar interactions at leading order. This is in contrast to spin-only moments where they appear only at higher order in perturbation theory.

[49] In this approximation, only the energy differences between atomic states with different charge configurations are retained. The splittings of the atomic manifold within each $4f^n$ configuration are ignored.

[50] J. C. Slater and G. F. Koster, Simplified LCAO method for the periodic potential problem, Phys. Rev. **94**, 1498 (1954).

[51] K. Takegahara, Y. Aoki, and A. Yanase, Slater-Koster tables for f electrons, J. Phys. C: Solid State Phys. **13**, 583 (1980).

[52] R. Finkelstein and A. Mencher, Interatomic electric quadrupole-quadrupole coupling in salts of cerium, J. Chem. Phys. **21**, 472 (1953).

[53] B. Bleaney, Quadrupole-quadrupole interaction in the rare earths, Proc. Phys. Soc. **77**, 113 (1961).

[54] Z. L. Dun, M. Lee, E. S. Choi, A. M. Hallas, C. R. Wiebe, J. S. Gardner, E. Arrighi, R. S. Freitas, A. M. Arevalo-Lopez, J. P. Attfield, H. D. Zhou, and J. G. Cheng, Chemical pressure effects on magnetism in the quantum spin liquid candidates $Yb_2X_2O_7$ (X = Sn, Ti, Ge), Phys. Rev. B **89**, 064401 (2014).

[55] L. D. C. Jaubert, O. Benton, J. G. Rau, J. Oitmaa, R. R. P. Singh, N. Shannon, and M. J. P. Gingras, Are Multiphase Competition and Order-by-Disorder the Keys to Understanding $Yb_2Ti_2O_7$? Phys. Rev. Lett. **115**, 267208 (2015).

[56] J. Robert, E. Lhotel, G. Remenyi, S. Sahling, I. Mirebeau, C. Decorse, B. Canals, and S. Petit, Spin dynamics in the presence of competing ferromagnetic and antiferromagnetic correlations in $Yb_2Ti_2O_7$, Phys. Rev. B **92**, 064425 (2015).

[57] J. des Cloizeaux, Extension d'une formule de Lagrange à des problèmes de valeurs propres, Nucl. Phys. **20**, 321 (1960).

[58] A. M. Hallas, J. Gaudet, M. N. Wilson, T. J. Munsie, A. A. Aczel, M. B. Stone, R. S. Freitas, A. M. Arevalo-Lopez, J. P. Attfield, M. Tachibana, C. R. Wiebe, G. M. Luke, and B. D. Gaulin, Phys. Rev. B **93**, 104405 (2016).